Title

Superimposed folding and W-Sn vein-type mineralisation in the Central Iberian Zone associated with late-Variscan oroclinal buckling: a structural analysis from the Regoufe area (Portugal)

Author names and affiliations (in correct order)

Dominique JACQUES[1]*

Philippe MUCHEZ[1]

Manuel SINTUBIN[1]

[1]KU Leuven, Department of Earth and Environmental Sciences, Geodynamics and Geofluids Research Group, Celestijnenlaan 200E, B-3001 Leuven, Belgium

* Corresponding author: tel. +32 16 327275 / dominique.jacques@kuleuven.be

Keywords

Type 3 fold interference

Cantabrian orocline

Granite-related ores

Cross-fold joint

Abstract

The Cantabrian orocline is a major orocline that bends the Variscan belt of Western Europe. Despite a wealth of studies, its timing and relationship with the late-Variscan folding stages in the Iberian Massif are still debated. This study provides an integrated structural analysis of the Variscan fold generations and associated W-Sn bearing vein systems within the southern Central Iberian Zone (Regoufe, Portugal), giving insight into their kinematic relationship with oroclinal buckling. Two superimposed fold generations with mutually parallel, steep to vertical fold axes have been identified. Isoclinal F_1 folds with E-W striking axial planes formed during coaxial shortening and are spatially localised. F_3 folds with NW-SE axial planes are associated with late-Variscan transpressional deformation and constrain the structural outline of the major folds. Temporal and kinematic considerations indicate that vertical-axis, asymmetric F_3 folding corresponds with the expected deformation style within the southern limb of the Cantabrian orocline. The Regoufe area is characterised by two types of W-Sn vein-type mineralisation. Granite-hosted hydrothermal quartz veins show a concentric distribution and are associated with the stress regime during granite emplacement. The vein system within the metasedimentary host rock, however, is emplaced along a regional, subhorizontal cross-fold joint system. This cross-fold joint system developed orthogonal to the subvertical F_3 fold axes, and is interpreted to be coeval with oroclinal buckling. These results impact the understanding of (i) the relative significance and geometry of the main deformation stages in the Iberian massif, reconciling the timing and kinematics of F_3 regional folding with oroclinal buckling, and (ii) the kinematic relationship between late- to postorogenic deformation and W-Sn vein-type mineralisation.

1. Introduction

The Variscan orogenic belt formed during the prolonged collision of Gondwana and Laurussia during the late Palaeozoic, constituting the European section of the Pangaea supercontinent (Matte, 2001; Nance et al., 2010; Kroner and Romer, 2013). The belt has a highly curved geometry, with the Ibero-Armorican arc as its most noticeable exponent (Weil et al., 2013; Ballèvre et al., 2014; Pastor-Galán et al., 2015b). The Iberian massif has been the main focal point to study the dynamics of this arcuate structure, since it contains the core of the arcuate structure, the Cantabrian orocline (Weil et al., 2013). In addition, the existence of a Central Iberian orocline, forming a S-shaped pair of isoclinal oroclines with the Cantabrian orocline (Fig. 1), has been suggested based on structural and paleocurrent data (Martínez Catalán, 2011, 2012; Shaw et al., 2012; Carreras et al., 2014). Such a S-shaped pair of coupled oroclines, however, is disputed by paleomagnetic and stratigraphic considerations (Pastor-Galán et al., 2015a, Dias et al., 2016).

Traditionally, crustal deformation in the Iberian massif has been considered the result of a long-lasting and diachronous deformation stage (D_1) of crustal shortening, with late-Variscan contraction (D_3) being only of local importance (Ribeiro et al., 1990; Abalos et al., 2002). This interpretation is in line with the geodynamic interpretation of the orocline resulting from the progressive indentation of Gondwana and Laurussia during collision (Brun and Burg, 1982; Matte, 1986; Quesada, 1991; Kroner and Romer, 2013). These considerations, however, have been challenged the last two decades by a multitude of studies that highlight the late-Variscan timing of orocline formation. A wealth of palaeomagnetic, structural and sedimentological data have inferred that the Variscan belt was quasi-linear prior to Late Carboniferous to Early Permian oroclinal buckling (ca. 310-297Ma) (Van der Voo et al., 1997; Weil et al., 2013; Fernández-Lozano et al., 2016; Pastor-Galán et al., 2015b, 2018). Furthermore, detailed structural analyses infer that the geometry of many large-scale fold structures in the Iberian massif have been strongly reshaped by late-Variscan D_3 deformation (Macaya, 1983; Martínez Catalán, 2012; Díez Fernández and Pereira, 2016; Dias da Silva et al., 2017; Pereira et al., 2017). To elucidate the above discrepancy, further studies tackling the geometry and kinematics of both Variscan fold generations are necessary.

Prior studies of the interference pattern between the F_1 and F_3 fold generations have mainly focused on the northern domains of the Iberian massif, in the core of the Cantabrian orocline (Fig. 1) (Julivert and Marcos, 1973; Bastida et al., 2010; Pastor-Galán et al., 2012). Within the Central Iberian Zone (CIZ), however, detailed accounts of F_1-F_3 superimposed folding are limited and have focused on narrow synforms containing Ordovician formations (Dias da Silva et al., 2017; Pastor-Galán et al., 2018).

In addition, the geometry of the different fold generations is disputed. On the one hand, Díez-Balda et al. (1990) subdivided the CIZ in two structural domains, based on significant differences in the D_1 deformation style: a northern 'Domain of Recumbent Folds' (DRF) and a southern 'Domain of Vertical Folds' (DVF) (Fig. 1). In the DRF, D_1 deformation is characterised by recumbent F_1 folds and low-angle thrusts in the upper structural levels, and fold-nappe stacks in the lower structural levels (Macaya et al., 1991; Díez Fernández et al., 2013). The F_1 folds are associated with a subhorizontal intersection lineation L_1. The DVF is characterised by F_1 folds with a subvertical axial planar S_1 foliation. Broad domains containing the Neoproterozoic-Cambrian basement are unconformably covered by narrow and tightly folded synclines where Ordovician (locally also Cambrian) to Upper Carboniferous metasedimentary rocks are outcropping (Abalos et al., 2002). F_1 folds show steep fold axes in the basement and mostly subhorizontal fold axes within the synclines (Díez-Balda et al., 1990). This discrepancy is related to the influence of pre-Variscan tilting of the Neoproterozoic formations during a Cadomian tectonothermal event (Talavera et al., 2015).

On the other hand, certain studies do not agree with the above subdivision and indicate that the entire CIZ is characterised by F_1 folds with subhorizontal fold axes (Dias and Ribeiro, 1994; Dias et al., 2016). The latter authors, however, mainly based their interpretation on the attitude of F_1 folds within the Ordovician of the tightly folded synclines, and not the Neoproterozoic-Cambrian basement.

These contrasting fold styles have also been suggested for the Regoufe area, part of the DVF (Fig. 1) and the subject of this paper: (i) mainly F_1 folds with subhorizontal axes, a monoclinic symmetry and a pervasive S_1 foliation (Dias et al., 2016), and (ii) asymmetric, kilometre-scale F_3 folds with subvertical fold axes and an axial planar S_3 crenulation cleavage that are refolding F_1 folds (Reavy, 1989; Valle Aguado et al., 2005). None of these studies, however, presented a detailed analysis of both fold generations. This is partly due to the monotonous nature of the Neoproterozoic basement, which makes a structural mapping of superimposed fold and foliation generations an arduous task.

The CIZ, moreover, hosts the majority of the Iberian W-Sn ore deposits, which are associated with widespread late- to postorogenic granitoids (Štemprok, 1981; Thadeu, 1989; Almeida et al., 2002; Neiva, 2002). The Regoufe area is known for the occurrence of several W-Sn deposits, as the region was the third Portuguese provider of tungsten during World War II (after Panasqueira and Borralha) (Moura, 2005). Besides many smaller exploitations, the district counts two main ore deposits, Minas de Regoufe and Minas de Rio de Frades, which are inactive since the mid 1950s (Correia et al., 2012). The different W-Sn bearing vein systems are cross-cutting the late-orogenic granite or the Neoproterozoic basement, showing a different geometry depending on the host rock (Sluijk, 1963). To our knowledge, the structural origin of the different W-Sn deposits and their relationship with the Variscan deformation structure has not been constrained.

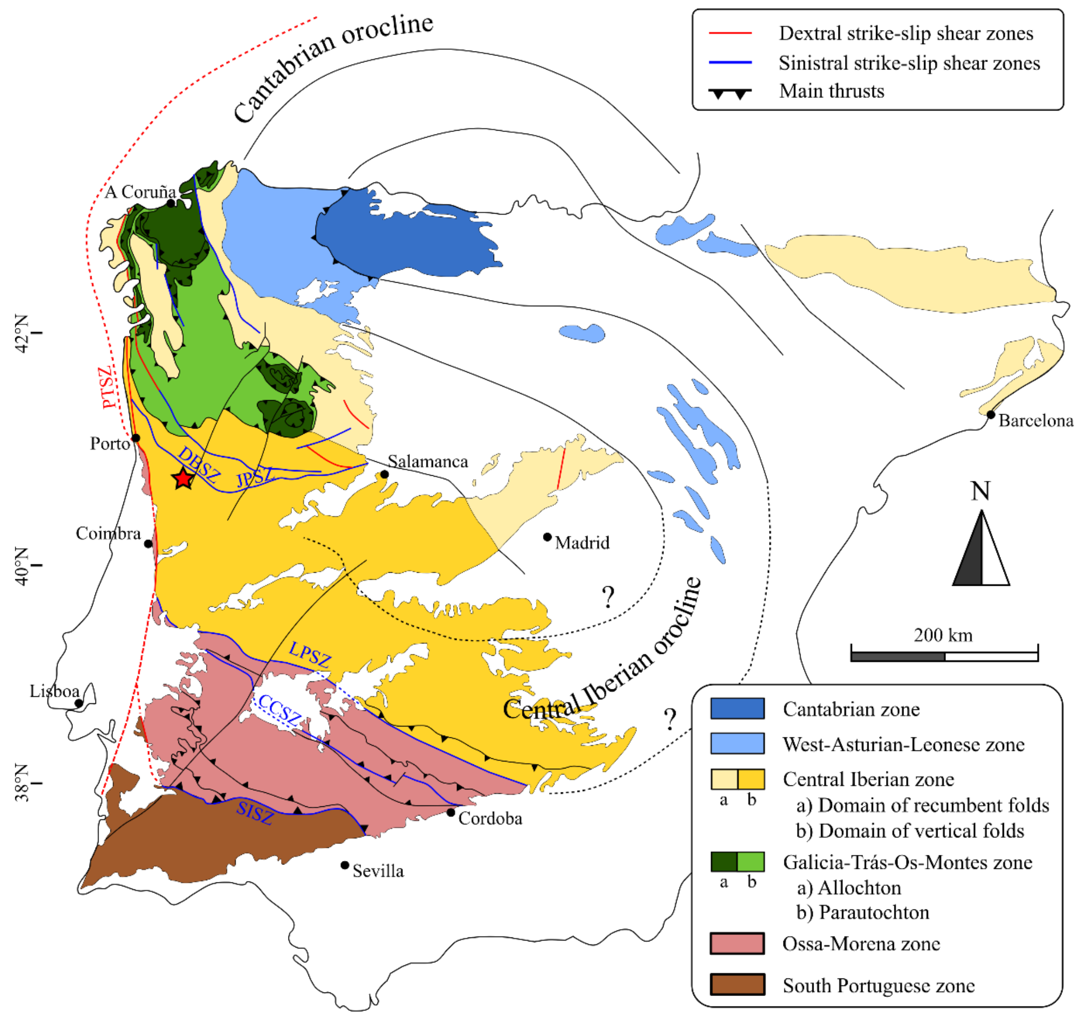

Fig. 1. Geological map of the Iberian massif showing the tectonostratigraphic zonation and the main Variscan structures. The study area is marked with a red star. The dashed black lines show the hypothesised outline of the Central Iberian orocline (Shaw et al., 2012). Adapted after Díez-Balda et al. (1990), Abalos et al. (2002) and Martínez Catalán et al. (2014). CCSZ: Coimbra-Cordoba Shear Zone; DBSZ: Douro-Beira Shear Zone; JPSZ: Juzbado-Penalva do Castelo Shear Zone; LPSZ: Los Pedroches Shear Zone; SISZ: Southern Iberian Shear Zone; PTSZ: Porto-Tomar Shear Zone.

The aim of this study is three-fold: (i) present a geometric and kinematic analysis of the F_1-F_3 fold generations, trying to delineate the geometry and significance of both deformation stages, (ii) investigate the kinematic relationship between W-Sn vein-type mineralisation and the Variscan deformation, and (iii) relate the observed structures to the kinematics of large-scale oroclinal buckling. An integrated approach is applied in which the geometry of the fold-foliation generations, a regional joint system and the W-Sn vein systems are correlated through a detailed orientation analysis. All data are plotted in the dip direction/dip and trend/plunge nomenclature, using the Stereonet 8 software (Cardozo and Allmendinger, 2013).

2. Geological setting

2.1. Geodynamic framework

The Iberian massif has traditionally been subdivided in six tectonostratigraphic zones, each reflecting a variable structural, stratigraphic and magmatic-metamorphic evolution: the Cantabrian, the West Asturian-Leonese, the Galicia-Trás-Os-Montes, the Central Iberian, the Ossa-Morena and the South Portuguese Zones (Fig. 1) (Lötze, 1945; Julivert et al., 1972; Farias et al., 1987). The CIZ is predominantly autochthonous and consists of metasedimentary rocks that were deposited at the northern border of Gondwana on an active and passive continental margin during the Neoproterozoic and Early Palaeozoic, respectively (Gutiérrez Marco et al., 1990; Orejana et al., 2015). The Neoproterozoic-Cambrian basement forms the main part of these sequences, consisting of a monotonous alternation of clay-, silt- and sandstones with local intercalations of volcanoclastics and conglomerates (de San José et al., 1990). In literature, these flyschoid sequences have been termed the 'Schist-Greywacke Complex' and 'Beira slates' (Ribeiro, 1990; Sequeira and de Sousa, 1991). The basement is unconformably overlain by narrow synclinal structures variably containing Lower Cambrian, Ordovician to Upper Carboniferous formations (Díez-Balda et al., 1990). Regional metamorphism ranges from lower greenschist to amphibolite facies (Martínez Catalán et al., 2014).

Two major angular unconformities are recognised in the CIZ: (i) one internally within the Neoproterozoic, and (ii) the aforementioned contact between the Lower Ordovician and the Neoproterozoic-Cambrian formations (Díez-Balda et al., 1990). The first unconformity is intra-Alcudian, separating the Lower and Upper Alcudian macro-units, and has been related to a

Cadomian tectonothermal event (ca. 560-550Ma) (Talavera et al., 2015). Moderate Cadomian folding, without any associated tectonic foliation or metamorphism, verticalised the Lower Alcudian (Talavera et al., 2015). Subsequently, the Upper Alcudian and Early Palaeozoic formations were deposited with a gentle stratification. The predominance of the Lower Alcudian throughout the southern CIZ (i.e. DVF) (Bouyx, 1970; Crespo and Rey, 1971; Ortega and González Lodeiro, 1986; Martín Herrero, 1989; de San José et al., 1990; Palero, 1993; López Díaz, 1995) explains the observed contrast in the plunge of the Variscan fold generations within the basement (steep to subvertical) and the synclines containing mainly Ordovician to Upper Carboniferous formations (moderate to subhorizontal) (Díez-Balda et al., 1990; Talevera et al., 2015).

Three Variscan, contractional deformation stages are traditionally considered to have affected the CIZ (Díez-Balda et al., 1990; Dallmeyer et al., 1997; Abalos et al., 2002). D_1 was active from the Late Devonian to Early Carboniferous (ca. 360-340Ma) and is reflected by F_1 folding and an associated penetrative, axial planar S_1 foliation. As mentioned, the geometry of the F_1 folds is suggested to vary strongly within the CIZ (Díez-Balda et al., 1990). D_2 (ca. 345-325Ma) mainly affected the northern part of the CIZ and is associated with strong non-coaxial, ductile flow along low-angle shear zones and a subhorizontal S_2 crenulation cleavage (Martínez Catalán et al., 1996, 2014; Rubio Pascual et al., 2013). This deformation stage is associated with the emplacement of the allochthonous and parautochthonous thrust sheets of the Galicia-Trás-Os-Montes Zone and related HP-metamorphism (Martínez Catalán et al., 2014; Arenas et al., 2016) (Fig. 1). After progressive thickening, thermal relaxation and gravitational destabilisation caused orogenic collapse with associated HT-LP metamorphism and the exhumation of migmatite domes along low-angle extensional detachments (Díez-Balda et al., 1995; Escuder Viruete et al., 1998; Arango et al., 2013; Díez Fernández et al., 2013). Renewed crustal thickening (D_3) was contemporaneous with transpressional deformation throughout the

Variscan belt (Kroner and Romer, 2013), active from the Middle to Late Carboniferous (ca. 315-305Ma) (Dallmeyer et al., 1997). Upright folds with a NW-SE striking, axial planar S_3 crenulation cleavage and associated strike-slip fault systems are testimony of this last deformation stage (Martínez Catalán et al., 2014). Simultaneously, the intrusion of granites and associated HT-LP metamorphism affected north and central Iberia (ca. 320-285Ma) (Fernández-Suárez et al., 2000).

2.2. Geology of the Regoufe area

The Regoufe area is located within the southeastern part of the Arouca municipality, part of the Aveiro district and about 50km to the southeast of Porto. The study area consists of three main geological entities: the Neoproterozoic-Cambrian Beira slate group, the late-orogenic Regoufe granite and a synclinal structure consisting of Ordovician and Upper Carboniferous metasedimentary rocks (Fig. 2). The Beira slates consist of a monotonous alternation of thin-bedded metapelites, metasiltstones and quartzitic sandstones. The pelites were transformed to slates and phyllites during lower greenschist regional metamorphism (Valle Aguado et al., 2005). The synclinal structure in the northern sector of the study area is part of the Porto-Sátão syncline that extends from Porto in the WNW to Sátâo in the ESE over a length of ca. 90km. The syncline has a steep isoclinal geometry and a general outcrop width of ca. 1-2km (Domingos et al., 1983). The northern border of the syncline has been related to a major shear zone, the Douro-Beira Shear Zone (DBSZ) (Fig. 1), which has been assigned both reverse and sinistral kinematics (Domingos et al., 1983; Valle Aguado et al., 2005). The contact between the Neoproterozoic Beira slates and the Ordovician formations in the syncline is an angular unconformity, as is clear from the orthogonal relationship between the S_0 traces and the syncline (Fig. 2).

The Regoufe granite is exposed over an area of ca. 6km² and is characterised by sharp contacts with the surrounding Beira slates. The coarse porphyritic two-mica granite consists of quartz, K-feldspar, albite, muscovite, biotite and minor tourmaline (Vriend et al., 1985). The K-feldspar megacrysts define a magmatic foliation that has a consistent subvertical NW-SE attitude (Fig. 2) (Sluijk, 1963). The Beira slates in its contact metamorphic aureole contain cordierite porphyroblasts. The aureole has an asymmetric distribution with a variable width (ca. 1km in the NE, ca. 3km in the SW) (Fig. 2). This asymmetry reflects the shape of the underlying granite, which is steep to the northeast and moderately-inclined to the southwest (Fig. 2 – profiles A-A' and B-B'). The latter is also reflected by the occurrence of subhorizontal to moderately-inclined granitic veins (Fig. 2). The coarse porphyritic texture and the presence of a subvertical NW-SE magmatic foliation, subparallel to the regional S_3 foliation, suggests that the Regoufe granite is part of the late- to postorogenic, strongly differentiated granite suite (Valle Aguado et al., 2005). W-Sn ore formation is spatially related to the occurrence of the Regoufe granite body. This relationship was confirmed by the trace element composition of the granite, which is extremely enriched in Sn, W, Li, Cs, P, Ta, Rb and F in comparison with similar low-Ca granites (Vriend et al., 1985). In addition, Van de Haar et al. (1993) demonstrated that the slates within the contact metamorphic aureole are enriched in Sn, F, B, W, Be, Cs and Rb relative to the average Beira slate composition.

Finally, the study area is delimited to the south by the Serra da Freita granite massif (Fig. 2), which forms part of a major synorogenic granite complex extending NW-SE from Porto to Viseu. Valle Aguado et al. (2005) dated the Serra da Freita granite at 308Ma, i.e. syn-D_3. The massif is associated with the sinistral Serra da Freita Shear Zone (Reavy, 1989).

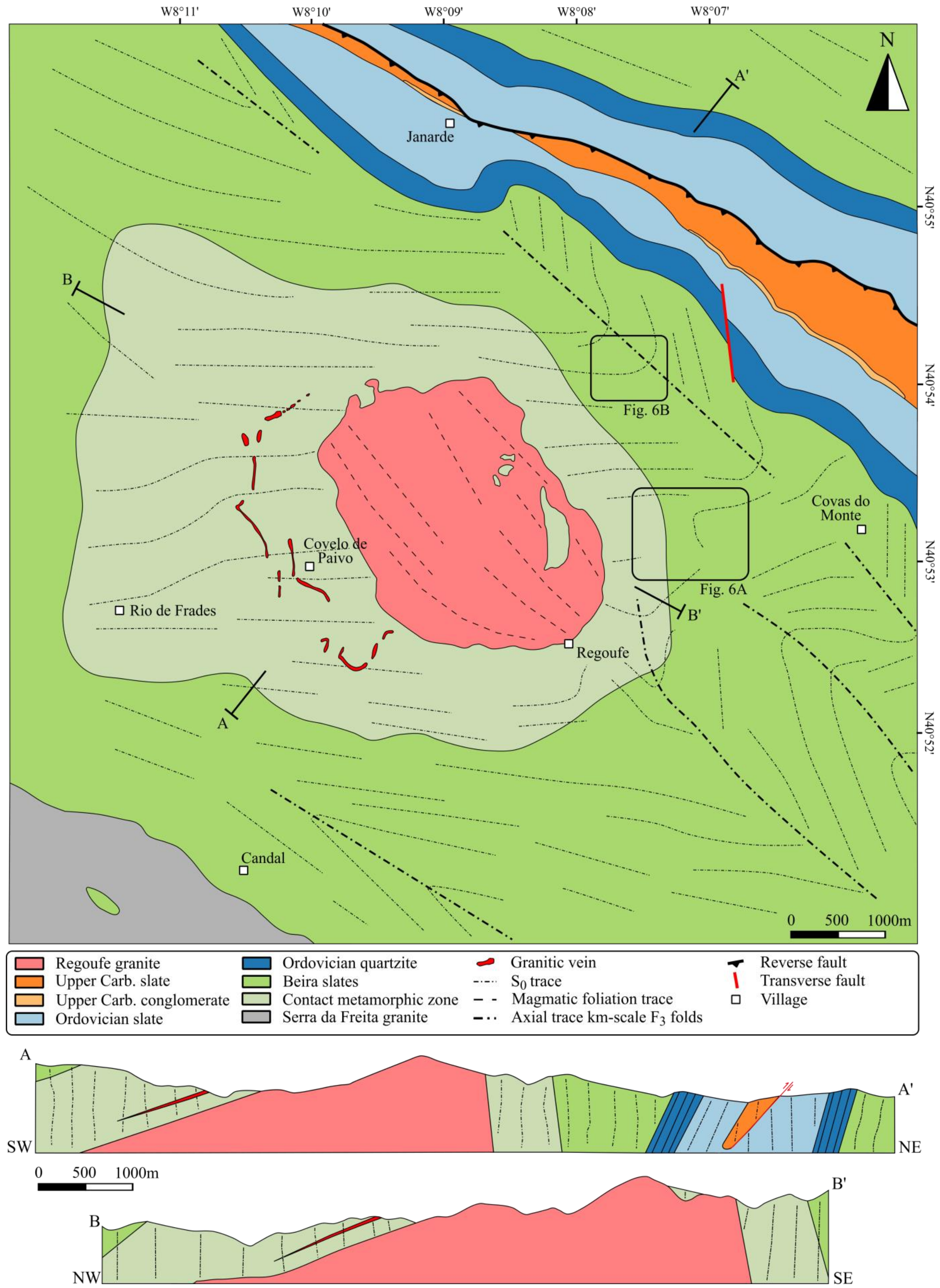

Fig. 2. Geological map of the Regoufe area and associated geological cross-sections (A-A') and (B-B'). The S_0 trace variation and the associated kilometre-scale F_3 folds are illustrated. The structure lines are based on our own structural analysis, complemented by the mapping results of Sluijk (1963). The orientation of the magmatic foliation within the Regoufe granite is adapted after Sluijk (1963).

3. Variscan deformation structure

3.1. Foliation generations

Structural mapping in the basement rocks over an area of ca. 25km² has highlighted the existence of two of the main regional foliation generations: S_1 and S_3. These tectonic foliations, in conjunction with S_0, have a consistent steep to subvertical orientation (Fig. 3A), as is characteristic for the Domain of Vertical Folds (DVF) (cf. Díez-Balda et al., 1990). The subhorizontal S_2 crenulation cleavage and associated shear zones were not observed, as is typical for the southern part of the CIZ (Díez-Balda et al., 1990). S_0 has a dip that varies between 50 and 90°, a variable strike with an E-W maximum and steeply plunging beta-axis (098/75) (Fig. 3A). S_1 is the main penetrative tectonic foliation, and is characterised by a strong preferred alignment of white mica and chlorite. Within the metapelites, S_1 forms a continuous slaty to phyllitic cleavage, while in the metasandstones an anastomosing, disjunctive cleavage is observed. S_1 is often subparallel to S_0, but in certain sectors of the Beira slates also displays a strong angular variation with S_0 and associated cleavage refraction (Fig. 3B). When not subparallel to S_0, S_1 is characterised by a clustered orientation distribution with a consistent subvertical, E-W striking attitude (average orientation of 181/86) (Fig. 3A). Within the Ordovician slates of the syncline, S_1 is also present as a slaty cleavage but consistently subparallel to S_0.

S_0 and S_1 are strongly crenulated by S_3, showing mm- to cm-scale (micro)folding (Figs. 3C-D). The S_3 crenulation cleavage is a spaced foliation (Figs. 3E-F), with spacing between cleavage domains varying from 50-200µm in metapelites to a minimum value of 100µm in metasandstones. S_3 has a consistent subvertical attitude and a NW-SE strike, with an average orientation of 065/84 (Fig. 3A). S_3 can be both symmetric (Fig. 3E) and asymmetric (Fig. 3F), depending on their position within the F_3 fold geometry (M-type vs. S- and Z-type parasitic folds).

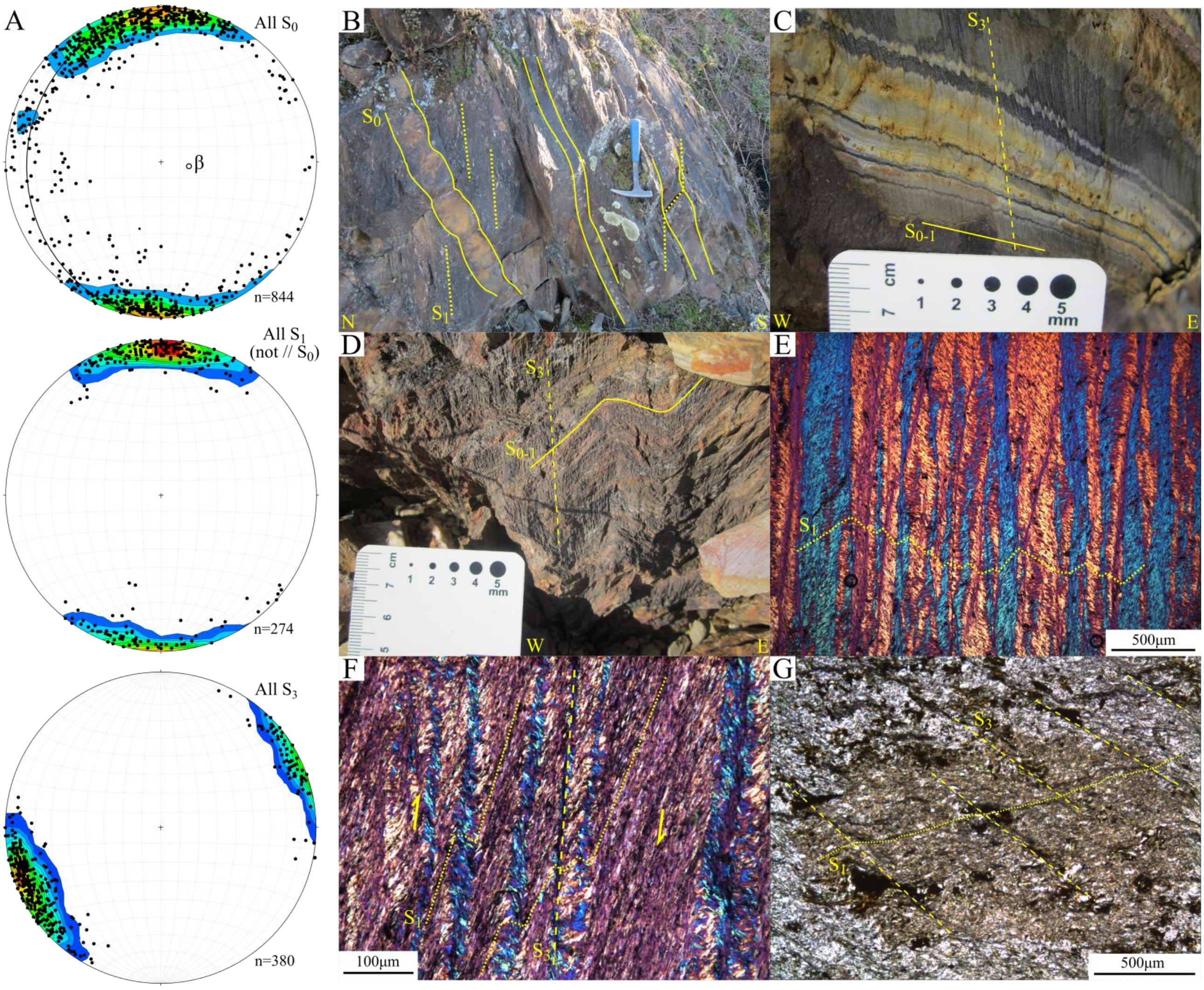

Fig. 3. Geometry of the different foliation generations. (A) Lower-hemisphere, equal-area stereographic projections of the poles to the S_0, S_1 and S_3 foliations. (B) Alternating metasandstone and metapelite beds that show S_1 cleavage refraction and boudinage. (C) Asymmetric crenulation of S_{0-1} by S_3. (D) Symmetric F_3 folding of S_{0-1} associated with an axial planar S_3 crenulation cleavage. (E-F) Micrographs with gypsum wedge illustrating the microfolding of S_1 by a zonal S_3 crenulation cleavage. The crenulation cleavage can be symmetric and asymmetric, respectively. (G) Fine-grained, strongly altered cordierite porphyroblast overgrowing the S_1 and S_3 foliations in the host rock.

The contact metamorphic aureole surrounding the Regoufe granite is characterised by a strong presence of cordierite porphyroblasts within the host rock. They are strongly altered to a fine-grained aggregate of white mica and chlorite (Fig. 3G), with only local remains of cordierite crystals being observed. The alignment of the cordierite porphyroblast spots is variable, from random to being oriented with the long axis subparallel to S_1 (Fig. 3G). The cordierites are overgrowing S_1 and S_3 (Fig. 3G), and thus result from mimetic overgrowth on these pre-existing foliations (cf. Passchier and Trouw, 2005).

3.2. Fold geometry

The F_1 and F_3 folds show a different spatial distribution. F_3 folds are omnipresent throughout large parts of the basement, while F_1 hinge zones are only visible at certain localities. S_0 has a dominant E-W strike, but there are strong variations to the north and east of the Regoufe granite (Fig. 2). In the latter zones, S_0 regularly has a subvertical, N-S to NNW-SSE striking attitude. This variability of S_0 reflects the presence of kilometre-scale, subvertical F_3 folds, whose axial planes are quite planar and continuous over large distances (Fig. 2). The presence of F_1 folds is not reflected by such a variability of S_0 on a kilometre-scale.

F_1 folds have an E-W striking axial plane, which is coincident with the S_1 foliation, and a fold axis that is plunging subvertical to steep to the east (Figs. 4A-C). All F_1 folds are of the symmetric M-type. The incompetent and competent lithologies in F_1 fold hinge zones show the typical divergent and convergent cleavage fans, respectively (Figs. 4B-C). Interlimb angles vary from relatively open (ca. 110° - Fig. 4A) to close (50-70° - Fig. 4B). The occurrence of the F_1 fold hinge zones is limited to specific locations, and throughout large parts of the study area, S_0 and S_1 are subparallel. These observations demonstrate the F_1 folds are approximately isoclinal. Only when approaching the hinge zones, an angular variation between S_0 and S_1 is apparent. F_1 folds are mostly limited to the areas to the west and northwest of the Regoufe granite, and between the Regoufe granite and Covas do Monte to the east (Fig. 2).

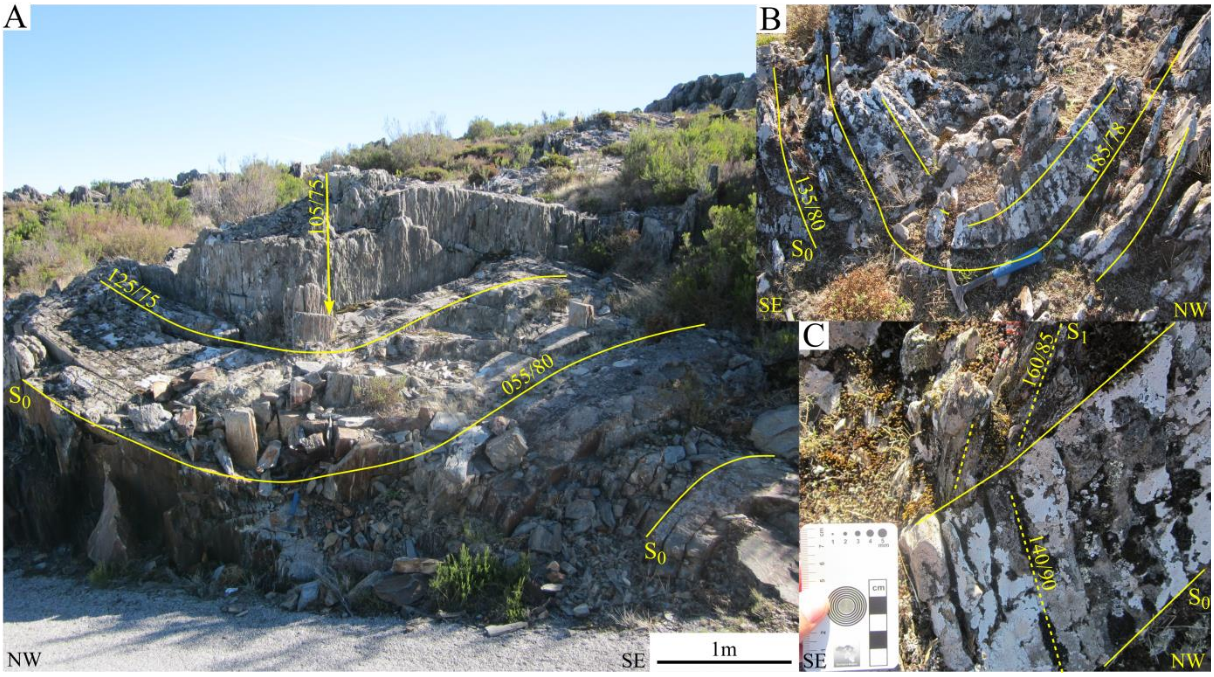

Fig. 4. Field photographs of the different fold generations. (A) Relatively open F_1 fold with subvertical S_0-S_1 intersection lineation and fold hinge line. (B) F_1 folds with a 50° interlimb angle. Hammer for scale (28cm). (C) Detailed view of S_1 cleavage refraction along metasandstone and slate beds in (C).

F_3 folds are observed where S_0 and S_1 are mutually subparallel or only show a slight angular variation, i.e. the F_1 fold limbs. They have a consistent NW-SE to NNW-SSE striking axial plane and a subvertical fold axis (Figs. 5A-B). F_3 folds also have a much more open geometry than the F_1 folds, with interlimb angles in the range of 80-120°. Depending on the orientation of the S_{0-1} fabric, F_3 folds show a different geometry. Symmetric M-type parasitic folds occur in the vicinity of larger-scale F_3 fold hinge zones (Fig. 5A). The dominant fold geometry, however, is asymmetric. If S_{0-1} has its typical E-W strike, F_3 folds are of the sinistral S-type. If S_{0-1} has a N-S to NE-SW strike, the F_3 folds are of dextral Z-type (Fig. 5B). The short limbs of the asymmetric F_3 folds typically have a length of 5-10m. Fig. 5C illustrates a schematic, plan-view diagram of this contrasting geometry of M-, S- and Z-type folds and how they relate with the S_{0-1} orientation.

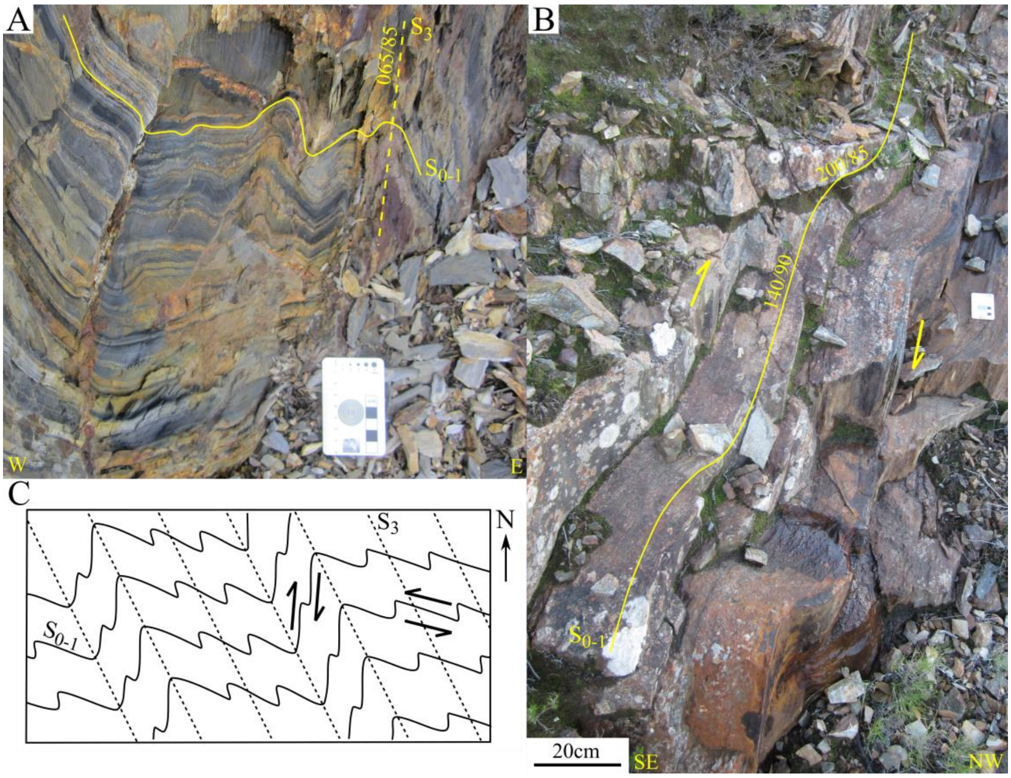

Fig. 5. (A) M-type parasitic F_3 folding of cm-scale laminations of alternating slate and metasiltstone. (B) Z-type, asymmetric F_3 folds with a strongly undulating S_{0-1}. (C) Plan-view sketch illustrating the relationship between the orientation of the subvertical S_{0-1} and S_3 foliations and the asymmetric mesoscale F_3 folds.

A detailed account of the regional geometry of the F_1 and F_3 fold generations is presented in the fold trace maps of Figs. 6A-B. Fig. 6A shows the nature of the F_1 and F_3 superimposed folding. Certain zones represent the hinge zones of large-scale F_1 folds and are characterised by S_1 having a consistent orientation at a high angle to S_0 (Fig. 6A), as was already shown in Figs. 4A-C. Other outcrops, representing the limbs of the large-scale F_1 folds where $S_0//S_1$, are strongly affected by asymmetric F_3 folding (Fig. 6A). Sinistral F_3 folds are predominant (Fig. 6A-B), since S_0 has a preferential E-W strike (Fig. 2). Locally, however, dextral F_3 folds are observed where S_0 has a deviating N-S to NNW-SSE-strike. To the northeast of the Regoufe granite (Fig. 6B), no obvious F_1 fold hinge zones are present. S_1 is consistently subparallel to S_0 and is strongly affected by F_3 folding, giving S_{0-1} an undulating geometry (Fig. 6B). Fig. 6B is situated across the axial plane of one of the major, kilometre-scale F_3 folds (Fig. 2), as is illustrated by the transition from a southern E-W to a northern NNE-SSW striking S_{0-1}.

4. Joint system

4.1. Geometry

The metasedimentary host rock is strongly cross-cut by a systematic joint system with a subhorizontal to locally moderately-inclined attitude, not exceeding 30° (Figs. 7A-C). One or more joint sets are present within a single outcrop, each consisting of mutually subparallel joints that are smooth, planar and regularly-spaced (Figs. 7A-C). The spacing and length of the joints varies with the affected lithology. Within fine-grained metapelites, the joints have a small spacing (10-50cm) and lengths up to several tens of metres (Figs. 7A-B). More competent host rocks (quartzitic sandstones), however, are characterised by joints that are less planar and locally anastomosing, have a larger spacing (>50cm) and a limited lateral continuity. Independent of the lithology, the joints are devoid of fractographic features (e.g. plumose structure). The joints also lack shear-related markers or lineations. In addition, all tectonic foliations (S_1, S_3) are cross-cut by the joints, but lack any displacement, i.e. just a dilational parting occurred. Hence, the joints should be considered as mode I extension fractures. The joints are typically barren, except in the vicinity of old galleries/exploitations, where subparallel quartz veins are observed (see further).

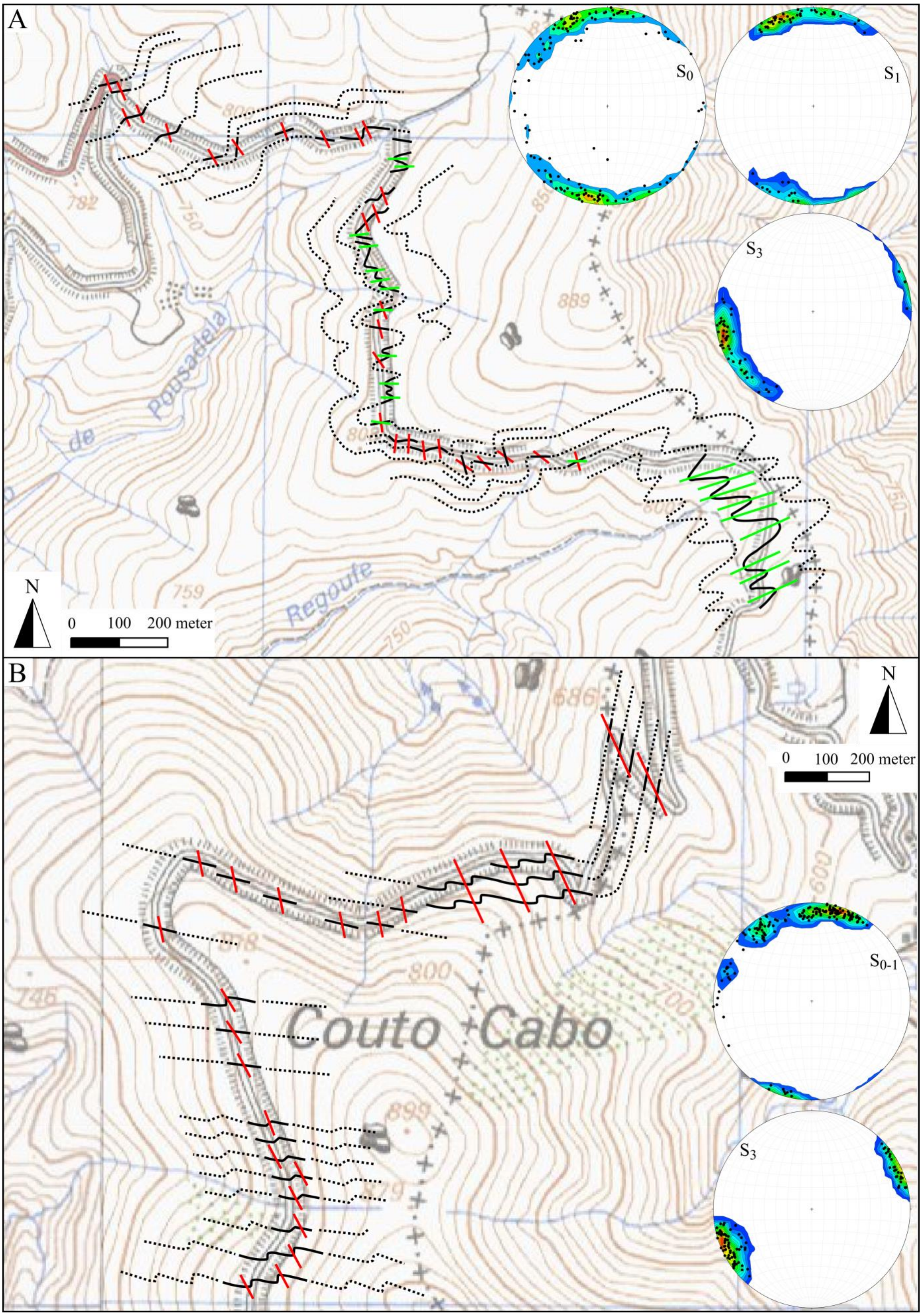

Fig. 6. Fold trace maps to the east of the Regoufe granite (cf. boxes in Fig. 2) that illustrate the geometry of F_1-F_3 superimposed folding (A) and F_3 folding (B). The black, green and red lines are marking the strike of

S_0, S_1 and S_3, respectively. The dotted lines are interpretative structure lines of S_0. Lower-hemisphere, equal-area stereographic projections of the poles to the measured S_0, S_1 and S_3 foliations are added.

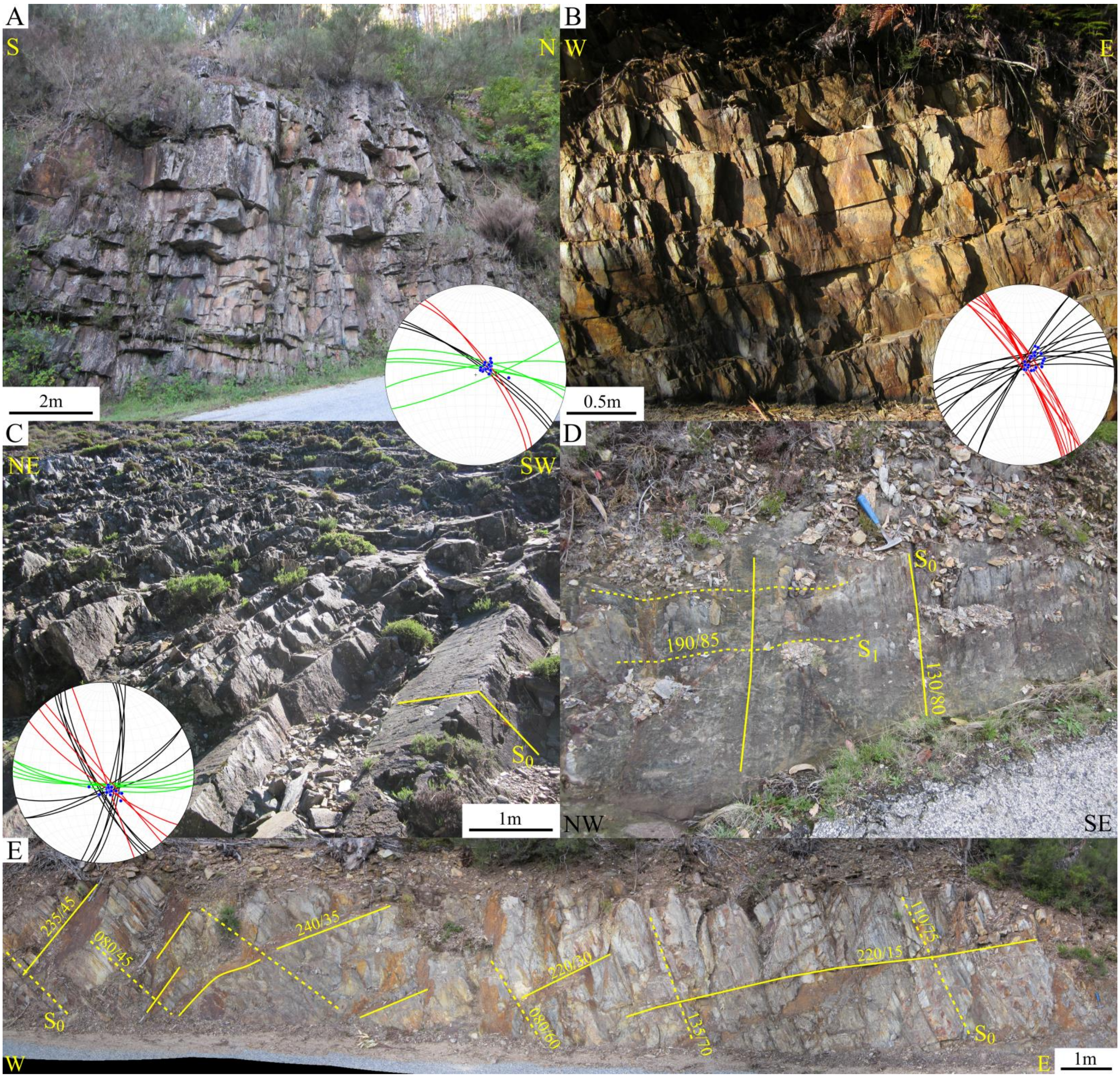

Fig. 7. Geometry of the joint system. The lower-hemisphere, equal-area stereographic projections show the poles to the joints (blue) and their relationship with the great circles of S_0 (black), S_1 (green) and S_3 (red). (A-B) Closely-spaced, subhorizontal joints in well-foliated slates. (C) Closely-spaced, moderately-dipping joints in alternating slates and metasandstones. (D) Outcrop, consisting of well-foliated slates, lacking the development of the S_3 foliation and the joint system. Hammer (28cm) for scale. (E) Outcrop that is characterised by alternating pelitic and quartzitic sandstone laminations that vary in dip from east to west. In the eastern part, S_0 has its typical subvertical attitude, while to the west S_0 gradually attains a lower dip. The orientation of the joints accordingly switches in attitude from east to west. In the east, the joints are subhorizontal, while in the west they are moderately-dipping in the opposite direction of S_0.

A mesoscale analysis demonstrates that the joint sets are consistently oriented at a high, suborthogonal angle relative to the S_0, S_1 and S_3 foliations and the associated intersection lineations (photographs and insets in Figs. 7A-C). As the orientation of the intersection lineations varies between the different outcrops, the joints follow a similar variation in dip direction and/or dip. This is especially well-illustrated in Fig. 7D, where S_0 changes its attitude within one single outcrop from subvertical to moderately-inclined. The joints maintain a suborthogonal orientation relative to S_0, changing from a subhorizontal to a moderately-inclined attitude, respectively. S_0-S_1 and $S_{0/1}$-S_3 intersection lineations are generally subparallel to each other in the study area, making it unclear at first sight to which fold generation the cross-fold joints are related. As stated, however, the study area is characterised by a predominant subparallel attitude of S_0 and S_1. Within outcrops that only contain an $S_{0/1}$-S_3 intersection lineation the presence of the joint system is pronounced (Fig. 7B). However, local outcrops that show a weak or undeveloped joint system are lacking an obvious S_3 crenulation cleavage (Fig. 7D). Based on these outcrop-scale observations it is suggested that the subhorizontal systematic joint sets can be defined as cross-fold or ac-joints (cf. Hancock, 1985), developing orthogonal to the mesoscale F_3 folds.

4.2. Orientation analysis

To verify this hypothesis, a regional orientation analysis of the joint system was performed, correlating its orientation with the geometry of the various foliations (S_0, S_1 and S_3) and their intersection lineations. A general comparison between the orientation distribution of the poles to the joints and the measured/calculated S_0-S_1 and $S_{0/1}$-S_3 intersection lineations indicates an excellent correlation, each having an average steep plunge to the east (Fig. 8A and Table 1). This steep plunge also corresponds with the beta-axis associated with the best-fit girdle of S_0 (098/75) (Fig. 3A). The pole figure coverage of the joint system shows the best accordance with the orientation distribution of the $S_{0/1}$-S_3 intersection lineations, showing a similar clustered distribution. In contrast, the S_0-S_1 intersection lineations show an E-W striking girdle distribution, which does not fully explain the joint poles plunging to the north and south (Fig. 8A).

For a more detailed correlation, the study area was subdivided in 9 zones characterised by joints with an average variation in dip direction (Fig. 8B). In zones F, G, H and I (western part of study area), the joints are dominantly dipping to the west and southwest (Fig. 8B and Table 1). To the east and northeast of the granite (zones C and D), the joint system has a preferential dip to the north (Fig. 8B and Table 1). To investigate these regional variations, the orientation distribution of the poles to the joints and the three foliations (left-hand side of Appendix A.1) was compared to the measured/calculated S_0-S_1 and $S_{0/1}$-S_3 intersection lineations and measured F_1 and F_3 fold hinge lines (right-hand side of Appendix A.1). The orientation analysis of all 9 zones demonstrates that the regional variability in the orientation of the joint system is controlled primarily by the attitude of the S_0 girdle. The poles to these S_0 girdles show a strong correlation with the average pole to the joint planes (Appendix A.1 and Table 1). The latter is especially apparent for those zones that show a strong preferred joint orientation, i.e. zones G, H and I with a S_0 girdle dipping to the west and southwest, or zones A and D with a S_0 girdle dipping to the northwest and north (Appendix A.1). S_1 and S_3 have a more consistent preferred orientation than S_0 throughout the study area. In zones F-I, however, S_3 has a preferred steep dip to the northeast, which correlates with the preferred dip to the west of the joint system (Appendix A.1).

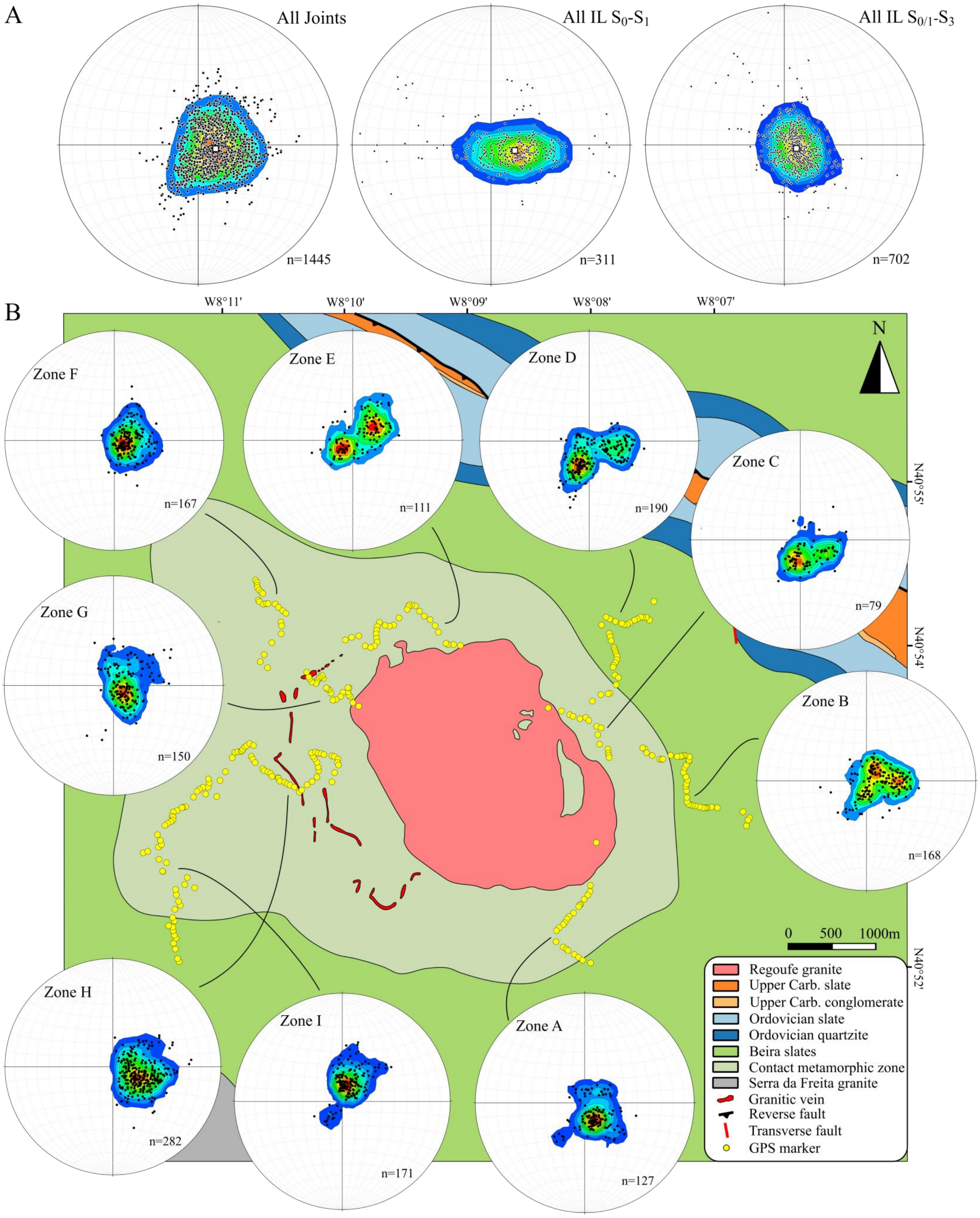

Fig. 8. Regional orientation analysis of the joint system. (A) Lower-hemisphere, equal-area stereographic projections of the poles to all joints and intersection lineations, both measured and calculated. The average orientations are marked with a white square. (B) Geological map incorporating the geographic position of

the different joint zones and the associated orientation distribution of the joint system. All stereoplots are lower-hemisphere, equal-area projections.

Also the orientation analysis indicates that the cross-fold joints are geometrically related to the F_3 folds and the associated. Firstly, this is illustrated by the strong correlation with the $S_{0/1}$-S_3 intersection lineations in zones C, D and I where the S_1 foliation is dominantly subparallel to S_0 and F_1 folds are lacking (Appendix A.1). Secondly, the correlation between the S_0-S_1 intersection lineations and the poles to the joints is very limited in zones B, F, G and H. The S_0-S_1 intersection lineations within these zones are either very dispersed or displays a E-W striking girdle, which is opposite to the preferred orientation of the joint poles (Appendix A.1). The $S_{0/1}$-S_3 intersection lineations, however, are characterised by a clustered distribution that strongly correlates with the joint orientation. Only zones A and E, where observed F_3 folding was rare, show a limited correlation between the $S_{0/1}$-S_3 intersection lineations and the joint poles.

To quantitatively assess these correlations, different spherical angles that relate the mean joint pole to the average orientation of the structural markers were calculated for each zone (Appendix A.2). The spherical angles comprise θ (relative to the pole to the best-fit girdle of S_0), ω_1 (relative to the mean S_0-S_1 intersection lineation), ω_2 (relative to the mean $S_{0/1}$-S_3 intersection lineation), φ_1 (relative to the average S_1) and φ_2 (relative to the average S_3). θ has an average value of 6.7 ± 5.6°, confirming a good correspondence between the calculated S_0 girdle and the average joint orientation for most zones (Appendix A.2). φ_1 and φ_2 are mostly greater than 80°, with mean spherical angles of 87.1 ± 2.3° and 85.4 ± 3.8°, respectively (Appendix A.2). Hence, a consistent suborthogonal relation exists between the joints and the tectonic foliations, despite the variability between the different zones. Similarly, ω_1 and ω_2 are dominantly smaller than 10° with means of 6.9 ± 3.5° and 4.6 ± 4.0°, respectively (Appendix A.2). Finally, to assess the randomness and cluster-girdle distribution of the orientation data the triangular plot introduced by Vollmer (1989) was applied (Appendix A.2), which uses the differences between the three eigenvalues of the orientation tensor. The joints, foliations (S_1 and S_3) and intersection lineations from zones A-I all show a strong clustered distribution, while S_0 is characterised by a (slight) girdle distribution (Appendix A.2).

Table 1. Orientation data for the 9 mapped joint zones in the Regoufe area. The table includes the average orientation of the joints, the pole to the best-fit girdle of S_0, the average orientation of the S_1 and S_3 tectonic foliations, and the average S_0-S_1 and $S_{0/1}$-S_3 intersection lineations. Also the average orientations for all 9 zones combined are added. All orientation data are indicated in dip direction/dip or trend/plunge.

	Zone A	Zone B	Zone C	Zone D	Zone E	Zone F	Zone G	Zone H	Zone I	All
Joints	322/12	277/09	332/13	346/12	232/07	273/11	268/09	285/22	200/15	283/10
β-axis S_0	158/81	088/80	122/83	133/78	075/70	096/68	090/65	096/62	053/74	098/75
S_1	192/81	177/87	160/80	/	176/88	178/87	186/87	186/86	341/84	181/86
S_3	030/83	068/82	075/88	065/86	076/77	069/79	068/84	051/85	054/83	065/84
IL S_0-S_1	146/79	101/76	100/71	/	100/78	098/74	102/69	103/75	040/69	102/76
IL $S_{0/1}$-S_3	170/89	080/82	144/84	136/79	059/79	091/79	120/81	114/78	017/82	106/83

5. Vein-type mineralisation

The Regoufe granite and the surrounding contact metamorphic slates are interspersed with a large number of old, small to moderate-sized open gallery exploitations of W-Sn quartz veins. In addition, aplite-pegmatite and granitic veins are also observed (Fig. 9). The veins are subdivided in two main groups, based on their host rock: (i) veins that are present within the Beira slates, and (ii) veins within the Regoufe granite body.

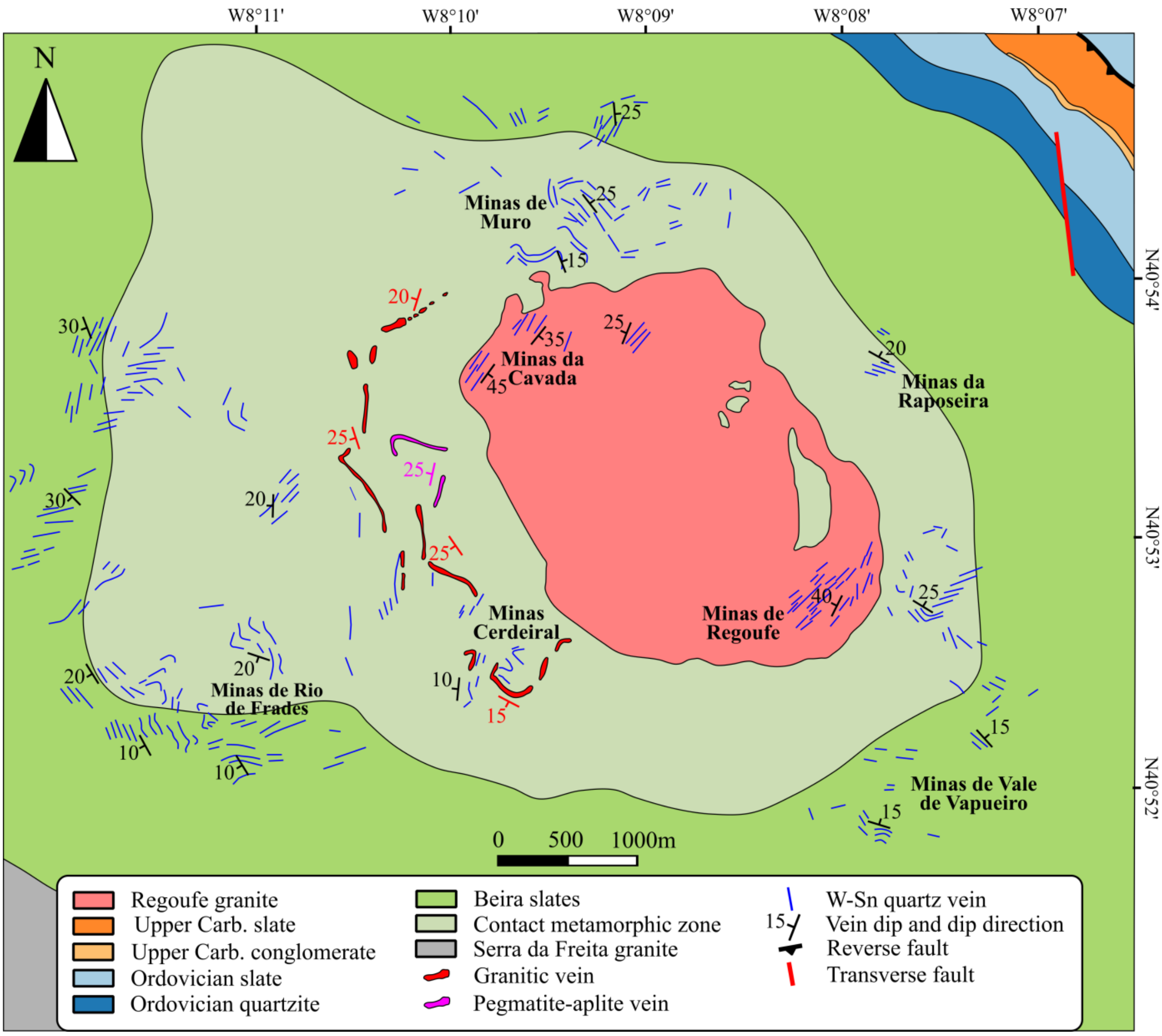

Fig. 9. Geological map illustrating the location and orientation of W-Sn quartz veins, pegmatite-aplite and granite veins. The vein orientations are based on own data and partly adapted after Sluijk (1963).

All W-Sn bearing hydrothermal quartz veins cross-cutting the Beira slates have a subhorizontal attitude (Fig. 9). The gangue mineralogy consists of quartz and minor muscovite. The wall rock surrounding the veins is often strongly enriched in tourmaline. The main ore minerals are wolframite and minor cassiterite. Wolframite crystals are prismatic and occur intergrown with blocky quartz crystals. Various minor sulphides (arsenopyrite, sphalerite, pyrite) are also reported (Sluijk, 1963). Although the old galleries have been strongly worked, the remnant veins that are observed have a thickness of 5-10cm (Fig. 10A). Neighbouring quartz veins are typically mutually subparallel, but significant variations in dip direction do occur across the study area (Fig. 9). Several observations demonstrate that the quartz veins are exploiting the regional joint system. Firstly, a consistent subparallel orientation was observed on the outcrop-scale (Fig. 10A). Secondly, the regional variation in vein orientation is concomitant with the changing attitude of the joint system surrounding the Regoufe granite. In the southwestern sector, the vein system is dipping ca. 10-30° to the west/southwest (Fig. 9). In the northeastern sector, however, the vein system is dipping ca. 15-25° to the east/northeast (Fig. 9). A similar bimodal orientation distribution, although slightly more variable, was witnessed for the cross-fold joint system (Fig. 8B).

Tabular aplite-pegmatite and granitic veins are consistently observed to cross-cut the Beira slates (Fig. 9). The veins occur predominantly along the western and southwestern border of the granite body, and lack W-Sn mineralisation (Fig. 9). The granite veins have a thickness that varies between 10 and 50m, and have a low to moderate dip to the west/southwest (15-30°, with a maximum of 40°) (Fig. 10B). They are interpreted to be subparallel with the underlying, low-dipping granite contact (Fig. 2 – profiles A-A' and B-B'). The granitic veins are composed mainly of large K-feldspar megacrysts in a matrix of fine-grained quartz, K-feldspar, plagioclase and muscovite. The aplite-pegmatite veins have a smaller thickness of ca. 1 to 3m, but are also dipping 10-25° to the west/southwest (Fig. 9). The aplite-pegmatites have a bimodal mineralogy, with the rim zone being composed of a fine-grained aplite and the core of the vein consisting of a coarse-grained pegmatite. The aplite has a typical fine-grained texture and consists dominantly of quartz and K-feldspar. The pegmatite has a more coarse-grained, crystalline texture with large euhedral crystals of K-feldspar (orthoclase and microcline), albite and quartz, interspersed with radiating muscovite booklets. These different magmatic veins again display a subparallel attitude with the neighbouring joint system, both on an outcrop-scale (Figs. 10B-D) and a regional scale (Fig. 9). Only the vein in Fig. 10D is for a certain length slightly discordant to the joint planes, switching between different joint planes from north to south. The average dip of ca. 15-30° to the west is in agreement with the preferential joint orientation of zone G (Fig. 8B).

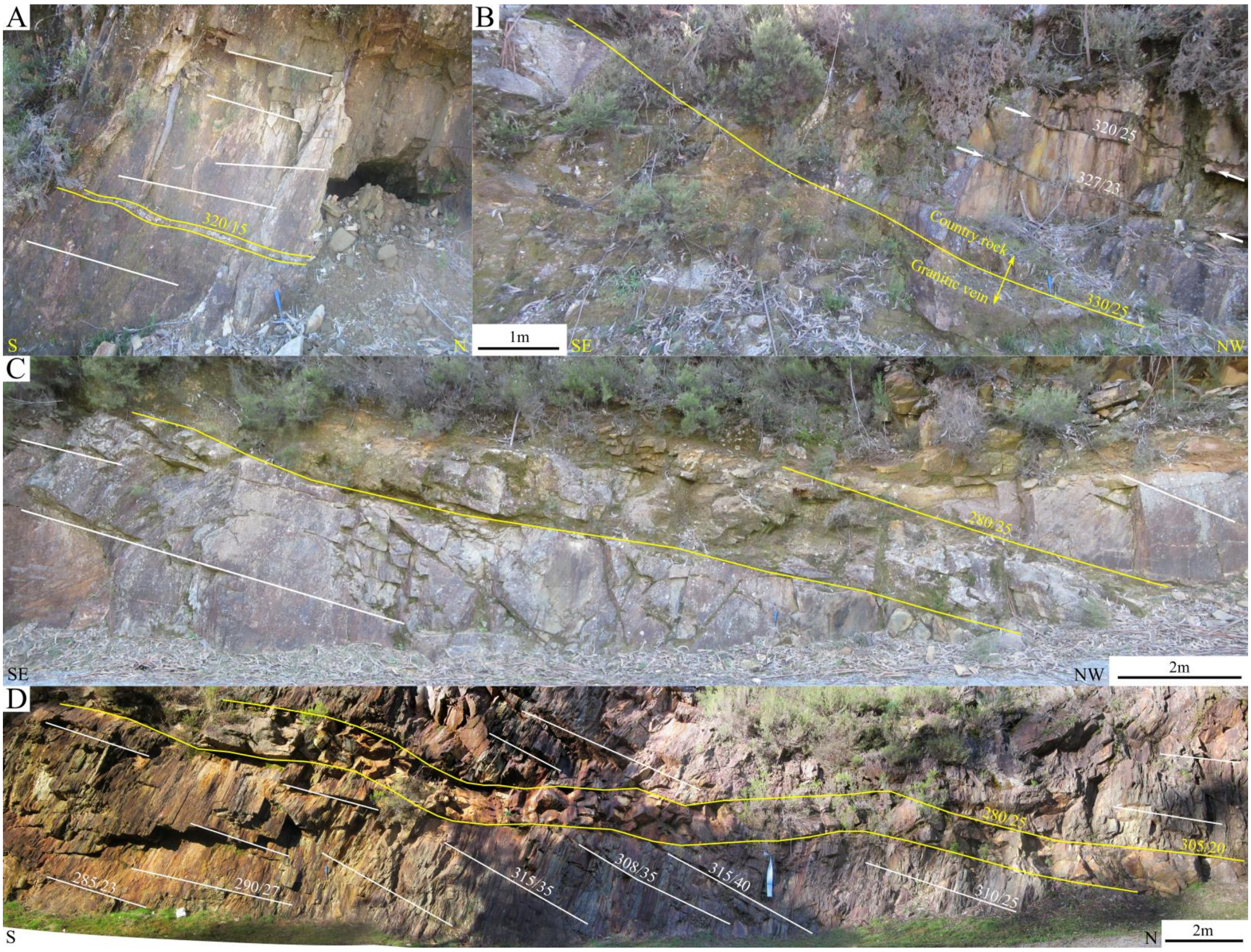

Fig. 10. Field photographs of W-Sn quartz veins, aplite-pegmatites and granitic veins. (A) Subhorizontal quartz vein subparallel to joints in the vicinity of a small exploitation. Hammer (28cm) for scale. (B) Granitic vein in the vicinity of Covelo de Paivo (Fig. 2). The vein has a moderate dip of ca. 25-30° to the west/northwest and is subparallel to joints within the metapelitic host rock. The joint planes are marked with white arrows. (C) Pegmatite of ca. 1.5m thick exploiting a joint set that is dipping slightly to the west. (D) Pegmatite exploiting subhorizontal to moderately-inclined joint sets, dipping to the west. In the central segment, the vein 'jumps' between different sets.

Granite-hosted, W-Sn bearing quartz veins were studied in two areas: (i) Minas de Regoufe at the southeastern extremity of the Regoufe granite, and (ii) Minas da Cavada at the northwestern border of the granite (Fig. 9). The Minas de Regoufe deposit consists of a group of subparallel veins, moderately-inclined to the northwest (average orientation of 280/39) (Fig. 11A). The Minas da Cavadas veins have a similar subparallel geometry and limited thickness. They are dipping moderately to the southeast (average orientation of 144/44) (Figs. 11B-C). Vein thickness is on average a few cm's. The granite host rock surrounding the veinlets is often altered to a quartz-muscovite greisen (1-5cm thick), with associated cassiterite, apatite and tourmaline (Sluijk, 1963). The ore mineralogy consists of wolframite and some cassiterite, while the gangue material consists of quartz. Unlike the veins present within the Beira slates, these granite-hosted veins do not appear to parallel a barren joint system.

Petrography of the all the different vein systems indicated that they are extension veins, as reflected by the growth directions of the gangue crystals orthogonal to the vein walls. Within hydrothermal quartz veins these consist of euhedral quartz crystals and fibrous mica-tourmaline crystals in wall rock selvages. Within the aplite-pegmatites large blocky feldspar crystals show growth at a high angle to the vein wall. Vein opening was syntaxial, as indicated by growth competition. Vein contacts are typically sharp and planar, and lack any shear-related phenomena.

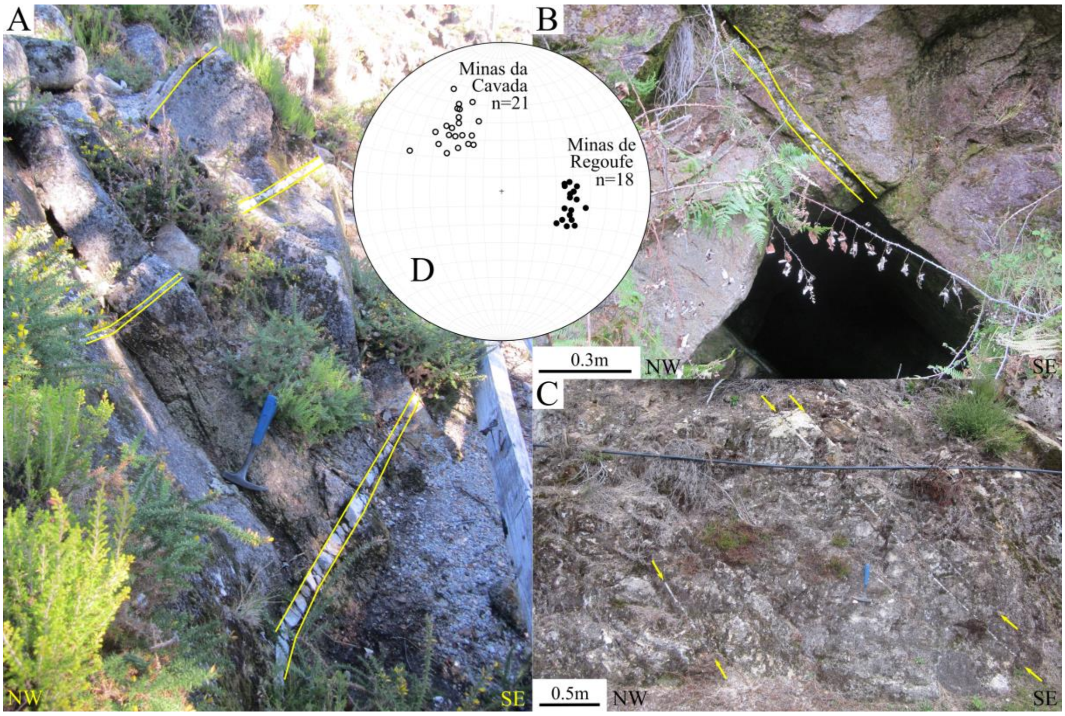

Fig. 11. Field photographs of granite-hosted hydrothermal quartz veins. (A) Subparallel veins at Minas de Regoufe with a moderate dip to the NW. Hammer (28cm) for scale. (B-C) Subparallel veins at Minas da Cavada, dipping moderately to the SE. (D) Lower-hemisphere, equal-area stereographic projection of the quartz vein poles at Minas de Regoufe and Minas da Cavada.

6. Interpretation and discussion

6.1. Fold interference model

To our knowledge, only Sluijk (1963) and Reavy (1988, 1989) have analysed the fold geometry in the study area up to now. Although the geological mapping by Sluijk (1963) acknowledged the subvertical fold axes, the F_1-F_3 and S_1-S_3 fold-foliation generations were not differentiated and one single deformation stage was interpreted. Reavy (1988, 1989) studied the Serra da Freita granite and the related D_3 sinistral shear zone to the south of the study area (Fig. 2). Near Rio de Frades, Reavy (1988, 1989) also described a secondary fold generation with subvertical fold axes, an associated NW-SE striking axial planar crenulation cleavage and a predominant sinistral asymmetry. In contrast to the observations in this study, however, he implied that the pre-existing F_1 folds with associated S_1 axial planar cleavage have a gentle plunge.

This study has highlighted the superposition of the regional F_1 and F_3 fold generations, which are associated with regional D_1 and D_3 deformation stages. The F_1 fold generation should not be considered as pre-Variscan since it is associated with a penetrative tectonic foliation, which did not develop in association with pre-Variscan deformation (Díez-Balda et al., 1990; Talavera et al., 2015). Taking into account the classification of Ramsay (1967), F_1-F_3 superimposed folding defines a type 3 interference pattern (Fig. 12A). Type 3 fold interference is characterised by successive fold generations with a small angle between their fold axes, and a high angle between their axial planes. Both the F_1 and F_3 fold axes are subvertical to steeply plunging to the east (Fig. 8A), the associated intersection lineations are subparallel at the outcrop-scale (Figs. 7A-C), and F_1 fold hinge lines lack a refolded/curved geometry. The S_1 and S_3 axial planar foliations show an average angular variation of 65° (average orientations of 181/86 and 065/84, respectively).

Based on the geometry of this fold interference pattern, the kinematics of the D_1 and D_3 deformation stage can be reconstructed. The F_1 fold generation consists of isoclinal folds with subvertical fold axes and an E-W striking axial plane, indicating a N-S maximum shortening direction during D_1 deformation (according to the current coordinates) (Fig. 12B). The F_1 isoclinal geometry and lack of any asymmetry suggests that D_1 shortening was largely coaxial, as suggested in literature (Abalos et al., 2002). The F_3 fold generation consists of subvertical folds with NW-SE striking axial planes and a higher interlimb angle than the F_1 folds (Fig. 12A). The superposition of these two fold generations results in the 3D and plan-view geometry pictured in Fig. 12A and Fig. 12C, respectively. While the axial planes of the F_1 folds become strongly curved and both S_0 and S_1 are folded, the F_1 fold hinges are not markedly affected by F_3 folding. The F_3 folds and associated S_3 foliation indicate a NE-SW maximum shortening, which is indeed typical for D_3 deformation (Díez-Balda et al., 1990; Abalos et al., 2002). The asymmetric F_3 fold style demonstrates a simple shear component, which is in correspondence with the transpressional D_3 deformation style and its association with numerous strike-slip fault systems and shear zones (Abalos et al., 2002).

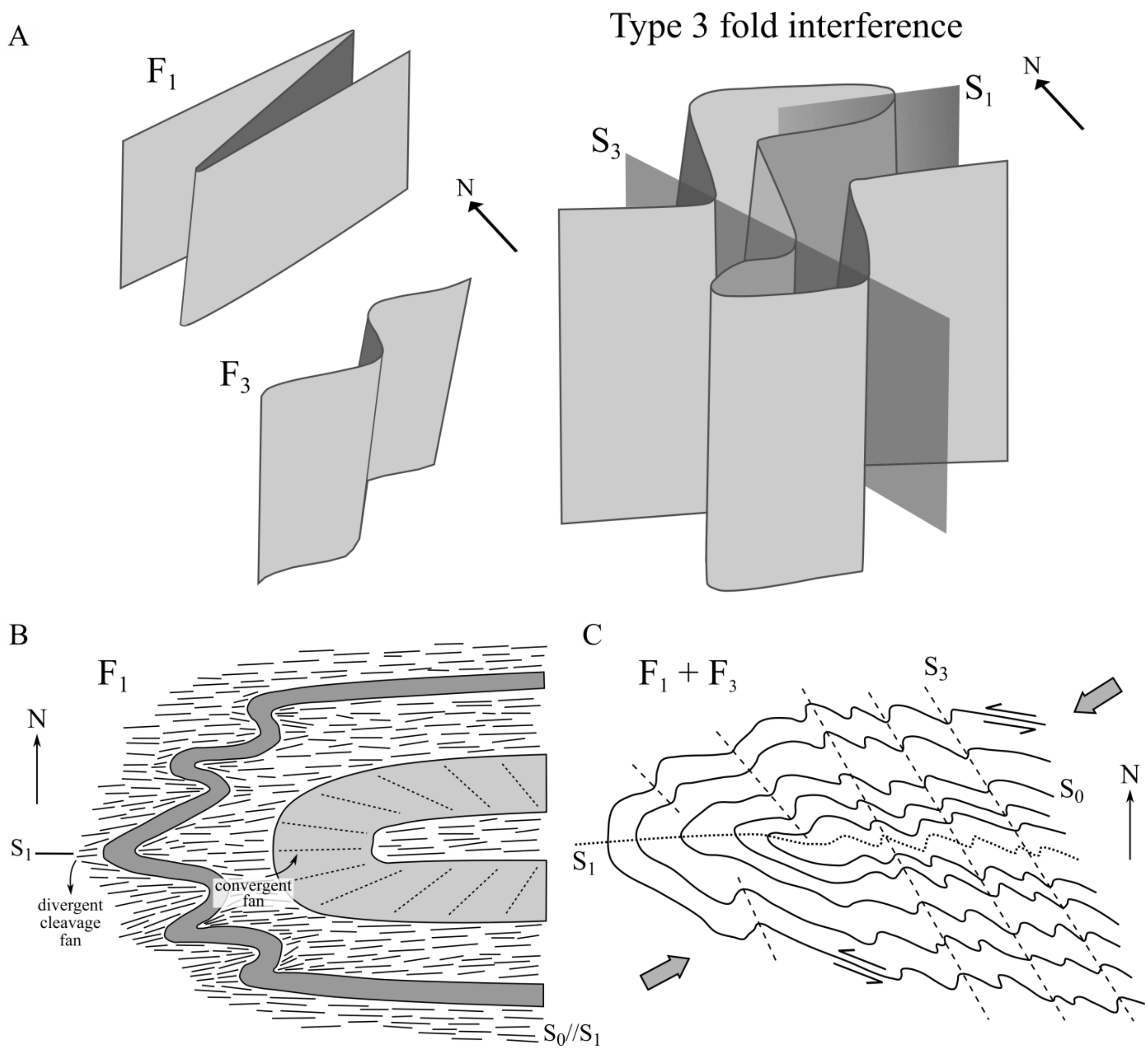

Fig. 12. Kinematic interpretation of the superimposed F_1 and F_3 fold generations. (A) Interpretative sketch of the fold interference pattern. The F_1 folds are isoclinal, subvertical folds with an E-W striking axial plane and fold limbs. The F_3 folds are asymmetric, subvertical folds with a NW-SE striking axial plane. Their superposition results in a type 3 interference geometry. (B) Plan-view sketch of the hinge zone of a F_1 fold. S_1 is subparallel to S_0 along the fold limbs, and only shows an angular variation with S_0 in the hinge zone. Modified after Passchier and Trouw (2005). (C) Plan-view sketch of a F_1 fold hinge zone after F_3 fold superposition. S_0 and S_1 in the fold limbs are strongly affected by asymmetric F_3 folding. The grey arrows delineate the maximum shortening direction.

6.2. Relative timing and mechanics of cross-fold jointing

The orientation analysis has demonstrated that the regional joint system has a consistent orthogonal orientation relative to the F_3 fold axes and the associated $S_{0/1}$-S_3 intersection lineations, i.e. they correspond to cross-fold joints. Firstly, this relationship is demonstrated by the strong development of the joint system in outcrops (Fig. 7B) and zones (e.g. zones C, F and I – Appendix A.1) where S_3 is present and S_0//S_1. In those localities where S_3 is lacking and a strong angular variation is observed between S_0 and S_1, the joint system is absent or weak (Fig. 7D and zones A and E – Appendix A.1). Secondly, we observed a stronger correlation between the clustered orientation distributions of the joint poles and the $S_{0/1}$-S_3 intersection lineations, while the S_0-S_1 intersection lineations show a girdle distribution (Fig. 8A and Appendix A.1). Had cross-fold joints indeed formed orthogonal to F_1 folds, they should have been strongly deformed and reactivated by subsequent deformation and F_3 folding. Instead, the cross-fold joint system shows great planarity, lateral continuity and a lack of shear deformation. Because F_1 and F_3 fold hinge lines are generally subparallel, a local correlation with the S_0-S_1 intersection lineation (e.g. zones A and E) is thus only apparent. Interestingly, these zones are situated along the long axis of the Regoufe granite (Fig. 8B). A possible explanation for the lack of penetrative S_3 development could be that zones A and E correspond to regional strain shadows, which are 'shielded' by the granite from D_3 deformation and associated NE-SW shortening.

The bimodal orientation distribution of the joint system is congruent with the asymmetric nature of the Regoufe granite (Fig. 2). Zones F-I are characterised by joint sets that are preferentially dipping to the west and southwest (Fig. 8B), which is approximately subparallel to the inferred low-angle granite contact and the associated granitic veins (Fig. 2). To the northeast, east and southeast of the Regoufe granite, where a steep contact is presented (Fig. 2), the correlation is less distinct. Zones C-D show joint sets that dip to the north and northeast, away from the granite body (Fig. 8B). Zones B and E, however, lack a preferred joint orientation, while in zone A the joints have a preferential dip to the north towards the granite contact. The above correlations do not suggest that the joints formed due to cooling or sagging of the underlying granite. If the joints had been granite-induced, they should display consistent orientations over large distances. Instead, the joints show a strict systematic variation in orientation on a meter-scale, when associated F_3 fold hinge lines change their attitude over tens of degrees, both in trend and plunge (Fig. 7E). The joints also do not correspond to sheeting joints that form in very superficial settings and have a more non-systematic and distinctly curved geometry (Martel, 2017). Instead, the geometric correlation is suggestive of (slight) doming by the Regoufe granite. Flexural deformation during doming is associated with the maximum principal stress being perpendicular to the granitic contact (Fig. 13A) (Gudmundsson, 2006). During expansion of the magma body and associated doming, the F_3 fold axes would act as material lines that maintain their initial orientation relative to the principal stress axes. Hence, their orientation would adapt from an initial subvertical orientation to an attitude orthogonal to the granite contact (Fig. 13B). Cross-fold jointing normal to these F_3 fold axes would show a large-scale orientation subparallel to the granite contact.

The orthogonal orientation between the joint system and F_3 fold axes indicates that F_3 folding was associated with hinge-parallel stretching. Some authors relate cross-fold joints to the earliest stages of folding and compressional deformation (Twiss and Moores, 1992; Reber et al., 2010), others consider them to form syn- to late-orogenic during layer-parallel shortening (Engelder, 1985; Hancock, 1985; Zhao and Jacobi, 1997; Fischer and Wilkerson, 2000), while another hypothesis assigns them a post-orogenic timing associated with the release of residual elastic strains (Reik and Currie, 1974; Engelder and Geiser, 1980; Weinberger et al., 2010). Ramsay and Huber (1987) indicated that joints are associated with very small strains, which suggest that the joints must form during the latest stages of an orogeny or are related to the posttectonic release of residual elastic strains. The observed cross-fold joint system indeed lacks any indications of ductile deformation or reactivation, confirming that they must be late- to post-D_3. In a similar manner, also the intrusion of the Regoufe granite appears to be a late-D_3 phenomenon. The granite shows a subvertical, NW-SE striking magmatic foliation (Sluijk, 1963), which is subparallel to S_3 and suggests a synchronicity between intrusion and D_3. The cordierite porphyroblasts within the contact metamorphic aureole surrounding the granite, however, are post-dating S_3 (Fig. 3G). The combination of these two observations indicates that granite intrusion most likely occurred during the final stage of D_3 (<305Ma), when the orogeny was already uplifted to upper-crustal depths (Gutiérrez-Alonso et al., 2015). Valle Aguado et al. (2005) indeed considered that the Regoufe granite was part of the late- to post-D_3 granite suite.

Despite their mutual late-D_3 origin, the exact relative timing between cross-fold jointing and granite intrusion is difficult to define due the lack of cross-cutting relationships. Nonetheless, it is argued that the cross-fold joints are pre- to syngenetic relative to the intrusion, having formed before/during doming and rotation of the F_3 fold axes. This sequence of events could explain the western low-angle contact of the granite. If pre- to syngenetic, the cross-fold joint system would have acted as a discontinuity influencing granite emplacement. This hypothesis is supported by the tabular granitic and aplite-pegmatite veins forming subparallel to the cross-fold joint system. Cross-fold jointing is largely coeval with late-D_3 intrusion of the Regoufe granite and subsequent magmatic-hydrothermal mineralisation.

6.3. Kinematics of veining

Magmatic-hydrothermal veins hosted by the Beira slates are exploiting the cross-fold joint system. The joints and veins have a consistent subparallel orientation in the field (Fig. 10), and barren joints are observed to be continuous past vein tips. Recently, the structural emplacement of W-Sn vein-type mineralisation at the world-class Panasqueira deposit, i.e. the most significant of the Iberian W-Sn deposits, was demonstrated to be controlled by a similar cross-fold joint system that developed orthogonal to the F_3 fold generation (Jacques et al., 2018). Unlike the observations at the Panasqueira deposit, however, outcrop-scale observations to delineate the relative timing and associated stress regime are lacking (e.g. segmentation structures, simultaneous opening of cross-cutting joint sets). It is not apparent whether the veins represent a later reactivation of the pre-existing joints or both formed cogenetic during F_3 folding (i.e. a local stress state with σ_3 subparallel to F_3 fold axes - Fig. 13B). Reactivation in a far-field contractional stress regime should, however, be discarded based on the analogy with the world-class Panasqueira deposit (Jacques et al., 2018) and the incompatibility with the D_3 transpressional deformation style. The subhorizontal extension veins must have lifted the lithostatic load and normal stress to the joint plane during dilation. Lithostatic fluid overpressures and small differential stresses (σ_1 - σ_3 < 4T, with T: tensile strength) were thus active during veining (cf. Boullier and Robert, 1992).

The W-Sn bearing quartz vein systems that are cross-cutting the Regoufe granite (i.e. Minas de Regoufe and Minas da Cavada - Fig. 9) are unrelated to the cross-fold joint system. These veins are moderately-inclined (ca. 40-50°) and form at a high angle to the Regoufe granite contact, i.e. a concentric orientation (Fig. 13A). This geometry is analogous to the dykes and inclined cone sheets (Gudmundsson, 2006; Magee et al., 2012), which form during the expansion of a central magma body and the associated increase in magmatic pressure. The emplacement of concentric dykes is classically associated with a compressional stress field that is characterised by a radial σ_1 and a σ_3 that is subparallel to the intrusion contact (Fig. 13A) (Anderson, 1936; Phillips, 1974). The quartz vein systems within the Regoufe granite are very limited in lateral continuity and do not propagate into the surrounding country rock. In addition, they are pure extension veins that lack shear deformation. Hence, it is suggested that they formed during the latest stages of internal fluid pressure increase, post-dating the main granite expansion phase and associated doming. During these latest stages, the strain rate and differential stresses decrease, allowing the formation of local hydraulic tension fractures (cf. Phillips, 1974). The relative timing of these granite-hosted quartz veins with the veins emplaced within the cross-fold joint system is unclear.

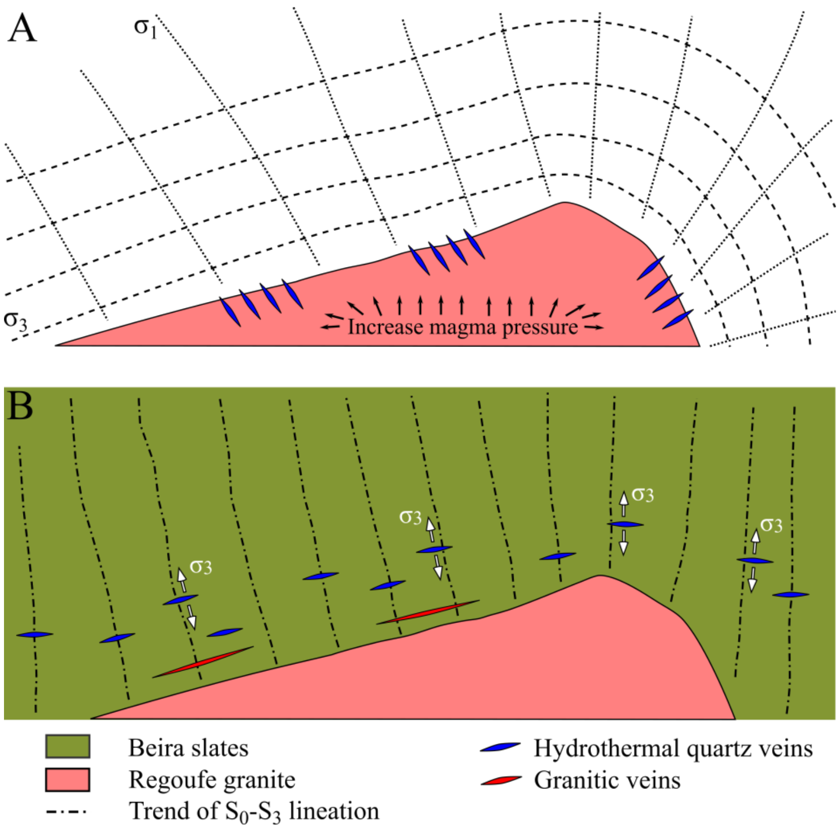

Fig. 13. Schematic line-drawings illustrating the contrasting stress regimes associated with veins emplaced within the Regoufe granite and the metasedimentary host rock. (A) The formation of concentric veins due to the expansion of the magma body and the associated increase in magmatic pressure. This doming of the magma body is also responsible for flexural deformation of the surrounding host rock. The dotted and dashed lines represent the trajectories of the maximum and minimum principal stresses surrounding the expanding intrusion. (B) The magmatic-hydrothermal veins emplaced within the metasedimentary host rock are exploiting the cross-fold joint system. This joint system is associated with a localised minimum principal stress σ_3 subparallel to F_3 fold axes.

6.4. Contribution to the geodynamic framework

Previous studies suggested Type 2 F_1-F_3 fold interference patterns in the Neoproterozoic basement of the southern part of the CIZ (DVF), consisting of a F_1 fold generation with subhorizontal fold axes that is overprinted by the F_3 fold generation with subvertical axes (Castro, 1986; Reavy, 1989). These authors, however, did not provide any direct field evidence on the F_1 fold geometry, but rather inferred subhorizontal F_1 fold axes based on the km-scale alternating synclines, while neglecting the Neoproterozoic basement rocks.

The presented F_1-F_3 fold interference model offers insight into the controversy surrounding the geometry of the F_1 and F_3 fold generations in the CIZ and the relative significance of the associated deformation stages. The F_1 folds in the Neoproterozoic-Cambrian basement are characterised by consistent subvertical fold axes, confirming similar results obtained in the Panasqueira area (Jacques et al., 2018). The notion that the entire CIZ is characterised by subhorizontal F_1 fold axes is incorrect, since in the DVF such a geometry only occurs within the narrow synclines unconformably overlying the broad Neoproterozoic domains. The contrast in plunge between the Variscan fold generations in the Neoproterozoic basement and the Early Palaeozoic formations is explained by pre-Variscan tilting of the Lower Alcudian (see above) (e.g. Talavera et al., 2015).

In addition, the significance of the F_3 fold generation, which defines the structural pattern within the Beira slates from an outcrop to a kilometre-scale, was highlighted. F_1 folds in the Regoufe area are of minor importance since their hinge zones are only locally observed and S_1 is generally subparallel to S_0. In the Panasqueira area, F_1 folds are similarly observed to be rare or lacking, while the asymmetric F_3 folds are defining the Variscan deformation geometry (Jacques et al., 2018). The axial traces of the large-scale F_3 folds (Fig. 2) are subparallel to the general strike of the Porto-Sátão syncline that is bordering the study area to the north (Fig. 2). These observations demonstrate that the syncline, mainly considered as a D_1 structure (Díez-

Balda et al., 1990; Abalos et al., 2002; Dias and Ribeiro, 1994; Dias et al., 2016), was strongly reshaped by the D_3 deformation stage. This conclusion is supported by the presence of the Upper Carboniferous (Stephanian C - Wagner and Álvarez-Vázquez, 2010) in the syncline (Fig. 2). The Upper Carboniferous was deposited syntectonically with the latest stage of D_3 (ca. 303-301Ma), but still shows a subvertical attitude and is cross-cut by a highly penetrative tectonic foliation (S_3) subparallel to the axial trace of the syncline (Sluijk, 1963; Domingos et al., 1983). Other studies in the Iberian massif have highlighted a similar interpretation from the structural analysis of superimposed folding (Julivert and Marcos, 1973; Pastor-Galán et al., 2012) and various major fold structures (Martínez Catalán, 2012; Díez Fernández and Pereira, 2016; Dias da Silva et al., 2017).

Up to now, the D_3 deformation stage and the formation of the Cantabrian orocline have been considered as unrelated phenomena. This was primarily due to a difference in relative timing. D_3 deformation has been dated at ca. 315-305Ma (Gutiérrez-Alonso et al., 2015; Valle Aguado et al., 2005), while oroclinal buckling has been constrained to ca. 310-297Ma (Pastor-Galán et al., 2015a). The incorporation of the Stephanian C metasediments within the F_3 Porto-Sátão syncline, however, suggests that the D_3 deformation stage was continuous till at least the Carboniferous-Permian boundary (ca. 300Ma). Hence, the previously suggested upper limit of D_3 deformation (305Ma) most likely represents the limit of ductile deformation. Beyond 305Ma, exhumation and erosion brought the orogen to upper-crustal depths where D_3 deformation and oroclinal buckling continued in the brittle realm.

The reported bending of the F_3 folds in the oroclinal hinge zone (Martínez Catalán, 2012) should not be considered as contradicting. Taking into account the tangential longitudinal strain distribution associated with the orocline (Gutiérrez-Alonso et al., 2008; Ries and Shackleton, 1976), the CIZ is part of its outer arc and should thus be characterised by stretching parallel and shortening orthogonal to the orogenic strike (cf. Gutiérrez-Alonso et al., 2004). F_3 folds developing coeval with oroclinal buckling would be expected to rotate along the outer arc hinge zone. Only within the inner arc, do F_3 folds need a radial orientation relative to the orogenic strike, which has been confirmed by studies of the superimposed folding pattern in the Cantabrian Zone (Julivert and Marcos, 1973; Pastor-Galán et al., 2012).

The observed F_3 fold style (Fig. 5C) is consistent with dextral transpression within the southern limb of the Cantabrian orocline, as expected from tangential longitudinal strain. This compatibility is demonstrated by a qualitative kinematic simulation of a dextral transpressional shear zone parallel to the strike of the CIZ (Fig. 14). Deformation within this transpressional shear zone is characterised by simultaneous pure and simple shear, internal rotation of the fabrics and a NE-SW maximum shortening direction at an angle of ca. 45° to the shear zone (Fig. 14), i.e. orthogonal to the axial plane of the Cantabrian orocline. Two asymmetric fold styles can form: (i) NW-SE to NNE-SSSW striking dextral Z-type F_3 folds if the initial foliation was oriented counterclockwise relative to the maximum shortening direction, or (ii) NE-SW to WNW-ESE striking sinistral F_3 S-type folds if the foliation was oriented clockwise. The latter F_3 fold style is conform the observed geometry in the Regoufe study area (i.e. red line in Fig. 14). The observed F_3 folds are thus interpreted to have formed during dextral transpression within the outer arc of the Cantabrian orocline. Consequently, the F_3 fold geometry is incompatible with the expected sinistral transpressional kinematics in the southern limb of the Central Iberian orocline (dotted lines in geological map of Fig. 14).

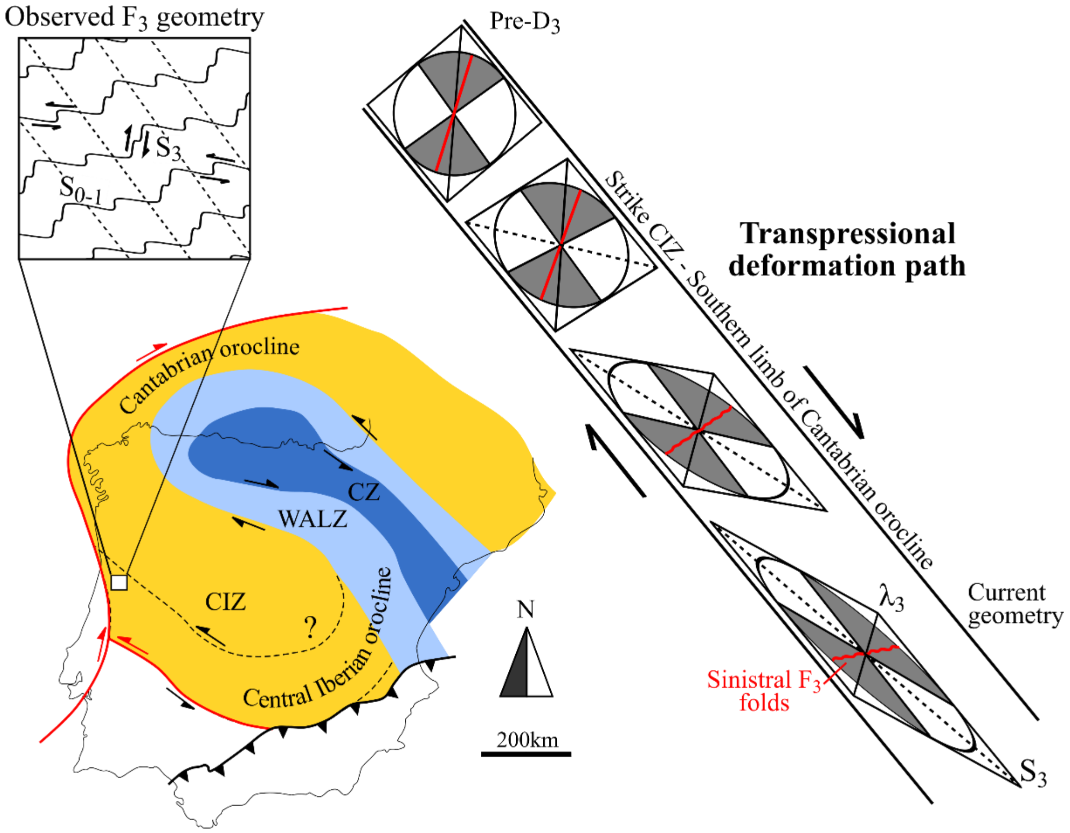

Fig. 14. Schematic line-drawings illustrating the observed F_3 geometry in the study area, its position on the geological map within the limbs of both the Cantabrian and Central Iberian oroclines, and a kinematic simulation of F_3 folding within a dextral transpressional shear zone of simultaneous pure and simple shear. The shear zone is subparallel to the strike of the CIZ and the southern limb of the Cantabrian orocline. The average orientation of S_{0-1} in the Regoufe area is marked with a red full line in the strain ellipsoids. The S_3 foliation is marked with a black dashed line.

7. Conclusions and perspectives

A structural analysis of fold-foliation generations in the Regoufe area has defined a model for F_1-F_3 superimposed folding in the southern CIZ based on detailed geological mapping and outcrop-scale observations. The fold interference model has given insight into the relative significance and geometry of both fold generations, enabling the evaluation of several discrepancies in literature. While F_1 folds appear to be more localised in nature than previously indicated, the F_3 fold generation is suggested to have shaped the major fold structures in the study area. Both fold generations have subvertical fold axes within the Neoproterozoic basement. The suggested fold interference model reconciles regional D_3 deformation and buckling of the Cantabrian orocline as coeval processes with similar kinematics. Vertical-axis F_3 folding within the outer arc of the orocline is in correspondence with the long-lasting model of a tangential longitudinal strain distribution associated with oroclinal buckling (Ries and Shackleton, 1976).

A kinematic interpretation of the different W-Sn ore deposits in the Regoufe area has been presented. Two modes of hydrothermal W-Sn mineralisation were recognised: (i) quartz veins exploiting a regional cross-fold joint system within the metasedimentary basement, and (ii) granite-hosted quartz veins that show a concentric orientation distribution and formed during granite emplacement and doming. The cross-fold joint system was previously also encountered in other study areas within the DVF, similarly localising W-Sn vein type mineralisation (Jacques et al., 2018). Hence, it is suggested that the joint system developed on a regional level throughout the DVF, coupled to the subvertical plunge of the F_3 fold generation. W-Sn mineralisation and oroclinal buckling appear to not only share their late-Variscan timing, but could also be considered as kinematically related processes. This working hypothesis and the geometry of the cross-fold joint system may function as an important tool in future mineral exploration endeavours.

Acknowledgements

This research is financially supported by research Grant OT/11/038 of the Onderzoeksfonds KU Leuven. D. Jacques was financially supported by the Agency for Innovation through Science and Technology (IWT).

References

Abalos, B., Carreras, J., Druguet, E., Escuder, J.V., Pugnaire, G.M.Z., Alvarez, S.L., Quesada, C., Fernández, L.R.R., Gil-Ibarguchi, J.I., 2002. Variscan and Pre-Variscan Tectonics. In: Gibbons, W., Moreno, M.T. (Eds.), The Geology of Spain. Geological Society of London, Special Publications, 155–183.

Almeida, A., Martins, H.C., Noronha, F., 2002. Hercynian Acid Magmatism and Related Mineralizations in Northern Portugal. Gondwana Research 5, 423–434.

Anderson, E.M., 1936. Dynamics of formation of cone-sheets, ring-dykes, and cauldron subsidence. Proceedings of the Royal Society of Edinburgh 56, 128–157.

Arango, C., Díez Fernández, R., Arenas, R., 2013. Large-scale flat-lying isoclinal folding in extending lithosphere: Santa Maria de la Alameda dome (Central Iberian Massif, Spain). Lithosphere 5, 483-500.

Arenas, R., Sánchez Martínez, S., Díez Fernández, R., Gerdes, A., Abati, J., Fernández-Suárez, J., Andonaegui, P., González Cuadra, P., López Carmona, A., Albert, R., Fuenlabrada, J.M., Rubio Pascual, F.J., 2016. Allochthonous terranes involved in the Variscan suture of NW Iberia: A review of their origin and tectonothermal evolution. Earth-Science Reviews 161, 140–178. doi:10.1016/j.earscirev.2016.08.010

Ballèvre, M., Martínez-Catalán, J.R., López-Carmona, A., Pitra, P., Abati, J., Fernández, R.D., Ducassou, C., Arenas, R., Bosse, V., Castineiras, P., Fernández-Suárez, J., Gómez Barreiro, J., Paquette, J.-L., Peucat, J.-J., Poujol, M., Ruffet, G., Sánchez Martínez, S., 2014. Correlation of the nappe stack in the Ibero-Armorican arc across the Bay of Biscay: a joint French-Spanish project. Geological Society of London, Special Publications, 77–113. doi:10.1144/SP405.13

Bastida, F., Aller, J., Pulgar, J.A., Toimil, N.C., Fernández, F.J., Bobillo-Ares, N.C., Menéndez, C.O., 2010. Folding in orogens: A case study in the northern Iberian Variscan belt. Geological Journal 45, 597–622. doi:10.1002/gj.1199

Boullier, A.-M., Robert, F., 1992. Palaeoseismic events recorded in Archaean gold-quartz vein networks, Val d'Or, Abitibi, Quebec, Canada. Journal of Structural Geology 14, 161–179.

Bouyx, E., 1970. Contribution à l'étude des formations anté-Ordoviciennes de la meseta meridionale (Ciudad Real et Badajoz). Memorias del Instituto Geológico y Minero de España 73, 263.

Brun, J.P., Burg, J.P., 1982. Combined thrusting and wrenching in the Ibero-Armorican arc: a corner effect during continental collision. Earth and Planetary Science Letters 61, 319–332. doi:10.1016/0012-821X(82)90063-2

Cardozo, N., Allmendinger, R.W., 2013. Spherical projections with OSXStereonet. Computers & Geosciences 51, 193–205.

Carreras, J., Druguet, E., 2014. Framing the tectonic regime of the NE-Iberian Variscan segment. In: Schulmann, K., Martínez Catalán, J.R., Lardeaux, J.M., Janousêk, V., Oggiano, G. (Eds.), The Variscan Orogeny: Extent, Timescale and the Formation of the European Crust. Geological Society, London, Special Publications 405, 249-264.

Castro, A., 1986. Structural pattern and ascent model in the Central Extremadura batholith, Hercynian belt, Spain. Journal of Structural Geology 8, 633–645. doi:10.1016/0191-8141(86)90069-6

Correia, V.F., Sá, A., Favas, P.J.C., 2012. Valorizaçáo patrimonial das Minas de Regoufe a Rio de Frades (Geoparque Arouca, Portugal). In: Henriques, M.H., Andrade, A.I., Quinta-Ferreira, M., Lopes, F.C., Barata, M.T., Pena dos Reis, R., Machado, A. (Eds.), Para Aprender Com a Terra - Memórias E Notícias de Geociências No Espaço Lusófono. Coimbra University Press.

Crespo, V., Rey, J., 1971. Contribución al estudio del Valle de Alcudia. Boletín Geológico y Minero 82, 512-515.

Dallmeyer, R.D., Martínez Catalán, J.R., Arenas, R., Gil Ibarguchi, J.I., Gutiérrez-Alonso, G., Farias, P., Bastida, F., Aller, J., 1997. Diachronous Variscan tectonothermal activity in the NW Iberian Massif: evidence from $^{40}Ar/^{39}Ar$ dating of regional fabrics. Tectonophysics 277, 307–337.

de San José, M.A., Pieren, A.P., García-Hidalgo, J.F., Vilas, L., Herranz, P., Peláez, J.R., Perejón, A., 1990. Central Iberian zone. Stratigraphy. Ante-Ordovician stratigraphy. In: Pre-Mesozoic Geology of Iberia, 147–159. Springer-Verlag, Berlin.

Dias, R., Ribeiro, A., 1994. Constriction in a transpressive regime: an example in the Iberian branch of the Ibero-Armorican arc. Journal of Structural Geology 16, 1543–1554. doi:10.1016/0191-8141(94)90032-9

Dias, R., Ribeiro, A., Romão, J., Coke, C., Moreira, N., 2016. Reviewing the arcuate structures in the Iberian Variscides; constraints and genetical models. Tectonophysics 681, 170–194. doi:10.1016/j.tecto.2016.04.011

Dias da Silva, Í., Gómez-Barreiro, J., Catalán, J.R.M., Ayarza, P., Pohl, J., Martínez, E., 2017. Structural and microstructural analysis of the Retortillo Syncline (Variscan belt, Central Iberia). Implications for the Central Iberian Orocline. Tectonophysics 717, 99–115. doi:10.1016/j.tecto.2017.07.015

Díez-Balda, M., Vegas, R., González-Lodeiro, F., 1990. Central Iberian zone. Autochtonous sequences. Structure. In: Dallmeyer, R.D., Martínez García, E. (Eds.), Pre-Mesozoic Geology of Iberia, 172–188. Springer-Verlag, Berlin.

Díez-Balda, M., Martínez Catalán, J.R., Ayarza Arribas, P., 1995. Syn-collisional extensional collapse parallel to the orogenic trend in a domain of steep tectonics: the Salamanca

Detachment Zone (Central Iberian Zone, Spain). Journal of Structural Geology 17, 163-182.

Díez Fernández, R., Gómez Barreiro, J., Martínez Catalán, J.R., Ayarza, P., 2013. Crustal thickening and attenuation as revealed by regional fold interference patterns: Ciudad Rodrigo basement area (Salamanca, Spain). Journal of Structural Geology 46, 115–128. doi:http://dx.doi.org/10.1016/j.jsg.2012.09.017

Díez Fernández, R., Pereira, M.F., 2016. Extensional orogenic collapse captured by strike-slip tectonics: Constraints from structural geology and U-Pb geochronology of the Pinhel shear zone (Variscan orogen, Iberian Massif). Tectonophysics 691, 290–310. doi:10.1016/j.tecto.2016.10.023

Domingos, L.C.G., Freire, J.L.S., Gomes da Silva, F., Gonçalves, F., Pereira, E., Ribeiro, A., 1983. The structure of the intramontane Upper Carboniferous basins in Portugal. In: de Sousa, M.J.L., Oliveira, J.T. (Eds.), The Carboniferous of Portugal. Memoriás dos Serviços de Portugal 29, 187–194.

Engelder, T., 1985. Loading paths to joint propagation during a tectonic cycle: an example from the Appalachian Plateau, U.S.A. Journal of Structural Geology 7, 459–476. doi:10.1016/0191-8141(85)90049-5

Engelder, T., Geiser, P., 1980. On the use of regional joint sets as trajectories of paleostress fields during the development of the Appalachian Plateau, New York. Journal of Geophysical Research 85, 6319–6341. doi:10.1029/JB085iB11p06319

Escuder Viruete, J., Hernáiz Huerta, P.P., Valverde-Vaquero, P., Rodríguez Fernández, R., Dunning, G., 1998. Variscan syncollisional extension in the Iberian Massif: structural, metamorphic and geochronological evidence from the Somosierra sector of the Sierra de Guadarrama (Central Iberian Zone, Spain). Tectonophysics 290, 87-109.

Farias, P., Gallastegui, G., González-Lodeiro, F., Marquínez, J., Martín Parra, L.M., Martínez Catalán, J.R., Pablo Macía, J.G. de, Rodríguez Femández, L.R., 1987. Aportaciones al conocimiento de la litoestratigrafia y estructura de Galicia Central. Memorias del Museo y Laboratorio Mineralógico y Geológico, Facultad de Ciencias, Universidad de Oporto 1, 411-431.

Fernández-Lozano, J., Pastor-Galán, D., Gutiérrez-Alonso, G., Franco, P., 2016. New kinematic constraints on the Cantabrian orocline: A paleomagnetic study from the Peñalba and Truchas synclines, NW Spain. Tectonophysics 681, 195-208.

Fernández-Suárez, J., Dunning, G.R., Jenner, G., Gutiérrez-Alonso, G., 2000. Variscan collisional magmatism and deformation in NW Iberia: constraints from U-Pb geochronology of granitoids. Journal of the Geological Society of London 157, 565–576. doi:10.1144/jgs.157.3.565

Fischer, M.P., Wilkerson, M.S., 2000. Predicting the orientation of joints from fold shape: Results of pseudo-three-dimensional modeling and curvature analysis. Geology 28, 15–18. doi:10.1130/0091-7613(2000)28<15:PTOOJF>2.0.CO

Gudmundsson, A., 2006. How local stresses control magma-chamber ruptures, dyke injections, and eruptions in composite volcanoes. Earth-Science Reviews 79, 1–31.

Gutiérrez-Alonso, G., Fernández-Suárez, J., Weil, A.B., 2004. Orocline triggered lithospheric delamination, in: Sussman, A.J., Weil, A.B. (Eds.), Orogenic Curvature: Integrating Paleomagnetic and Structural Analyses. Geological Society of America Special Paper 383. Geological Society of America, pp. 121–131.

Gutiérrez-Alonso, G., Fernández-Suárez, J., Weil, A.B., Murphy, J.B., Nance, R.D., Corfu, F., Johnston, S.T., 2008. Self-subduction of the Pangaean global plate. Nature Geoscience 1, 549–553.

Gutiérrez-Alonso, G., Collins, A.S., Fernández-Suárez, J., Pastor-Galán, D., González-Clavijo, E., Jourdan, F., Weil, A.B., Johnston, S.T., 2015. Dating of lithospheric buckling: $^{40}Ar/^{39}Ar$ ages of syn-orocline strike-slip shear zones in northwestern Iberia. Tectonophysics 643, 44–54. doi:10.1016/j.tecto.2014.12.009

Gutiérrez Marco, J.C., de San José, M.A., Pieren, A.P., 1990. Central Iberian zone. Autochthonous sequences. Post-Cambrian Palaeozoic Stratigraphy. In: Pre-Mesozoic Geology of Iberia, 160–171. Springer-Verlag, Berlin.

Hancock, P.L., 1985. Brittle microtectonics: principles and practice. Journal of Structural Geology 7, 437–457.

Jacques, D., Vieira, R., Muchez, P., Sintubin, M., 2018. Transpressional folding and associated cross-fold jointing controlling the geometry of post-orogenic vein-type W-Sn mineralization: examples from Minas da Panasqueira, Portugal. Mineralium Deposita 53, 171-194. doi:10.1007/s00126-017-0728-6

Julivert, M., Fontboté, J.M., Ribeiro, A., Conde, L., 1972. Mapa Tectónico de la Península Ibérica y Baleares E. 1:1.000.000. Instituto Geológico y Minero de España, Madrid.

Julivert, M., Marcos, A., 1973. Superimposed folding under flexural conditions in the Cantabrian zone (Hercynian Cordillera, northwest Spain). American Journal of Science 273, 353–375.

Kroner, U., Romer, R.L., 2013. Two plates — Many subduction zones: The Variscan orogeny reconsidered. Gondwana Research 24, 298–329. doi:10.1016/j.gr.2013.03.001

López Díaz, F., 1995. Late Precambrian series and structures in the Navalpino Variscan anticline (Central Iberian Peninsula). Geologische Rundschau 84, 151-163.

Lötze, F., 1945. Zur Gliederung der Varisziden der Iberischen Meseta. Geotektonische Forschungen 6, 78–92.

Macaya, J., 1983. Bandas miloníticas plegadas en los materiales metamórficos del sur de Segovia. Studia Geologica Salmanticensia XVIII, 93–106.

Macaya, J., González-Lodeiro, F., Martínez-Catalán, J.R., Alvarez, F., 1991. Continuous deformation, ductile thrusting and backfolding of cover and basement in the Sierra de Guadarrama, Hercynian orogen of central Spain. Tectonophysics 191, 291–309. doi:http://dx.doi.org/10.1016/0040-1951(91)90063-X

Magee, C., Stevenson, C., O'Driscoll, B., Schofield, N., McDermott, K., 2012. An alternative emplacement model for the classic Ardnamurchan cone sheet swarm, NW Scotland, involving lateral magma supply via regional dykes. Journal of Structural Geology 43, 73–91. doi:10.1016/j.jsg.2012.08.004

Martel, S.J.., 2017. Progress in Understanding Sheeting Joints over the Past Two Centuries. Journal of Structural Geology 94, 68–86. doi:10.1016/j.jsg.2016.11.003

Martín Herrero, D., 1989. Los materiales Precámbrico-Cámbricos al O y S de Ciudad Rodrigo (Salamanca): series, discordancias y correlaciones. Boletín Geológico y Minero 100, 167-177.

Martínez Catalán, J.R., 2011. Are the oroclines of the Variscan belt related to late Variscan strike-slip tectonics? Terra Nova 23, 241-247.

Martínez Catalán, J.R., 2012. The Central Iberian arc, an orocline centered in the Iberian Massif and some implications for the Variscan belt. International Journal of Earth Sciences 101, 1299–1314. doi:10.1007/s00531-011-0715-6

Martínez Catalán, J.R., Arenas, R., Díaz García, F., Abati, J., 1996. Variscan accretionary complex of northwest Iberia: terrane correlation and succession of tectonothermal events. Geology 25, 1103–1106.

Martínez Catalán, J.R., Rubio Pascual, F.J., Díez Montes, A., Díez Fernández, R., Gómez

Barreiro, J., Dias Da Silva, I., González Clavijo, E., Ayarza, P., Alcock, J.E., 2014. The late Variscan HT/LP metamorphic event in NW and Central Iberia: relationships to crustal thickening, extension, orocline development and crustal evolution. Geological Society of London, Special Publications 405, 225–247. doi:10.1144/SP405.1

Matte, P., 2001. The Variscan collage and orogeny (480 - 290 Ma) and the tectonic definition of the Armorica microplate : a review. Terra Nova 13, 122–128.

Matte, P., 1986. Tectonics and plate tectonics model for the Variscan belt of Europe. Tectonophysics 126, 329–374.

Moura, A., 2005. Valorização do património geomineiro da Serra da Freita. In: Actas Do IV Seminário de Recursos Geológicos, Ambiente E Ordenamento Do Território, Universidade de Trás-os-Montes e Alto Douro, E1–E5.

Nance, R.D., Gutiérrez-Alonso, G., Keppie, J.D., Linnemann, U., Murphy, J.B., Quesada, C., Strachan, R., Woodcock, N.H., 2010. Evolution of the Rheic Ocean. Gondwana Research 17, 194–222. doi:10.1016/j.gr.2009.08.001

Neiva, A.M.R., 2002. Portuguese granites associated with Sn-W and Au mineralizations. Bulletin of the Geological Society of Finland 74, 79–101.

Orejana, D., Merino Martínez, E., Villaseca, C., Andersen, T., 2015. Ediacaran – Cambrian paleogeography and geodynamic setting of the Central Iberian Zone : Constraints from coupled U – Pb – Hf isotopes of detrital zircons Ediacaran – Cambrian paleogeography and geodynamic setting of the Central Iberian Zone : Constraints. Precambrian Research 261, 234–251. doi:10.1016/j.precamres.2015.02.009

Ortega, E., González Lodeiro, F., 1986. La discordancia intra-Alcudiense en el dominio meridional de la Zona Centroibérica. Breviora Geológica Astúrica 27, 27-32.

Palero, F.J., 1993. Tectónica pre-hercínica de las series infraordovícicas del anticlinal de

Alcudia y la discordancia intraprecámbrica en su parte oriental (sector meridional de la Zona Centroibérica). Boletín Geológica y Minero 104, 227-242.

Passchier, C.W., Trouw, R.A.J., 2005. Microtectonics. Springer-Verlag, Berlin.

Pastor-Galán, D., Dias da Silva, I.F., Groenewegen, T., Krijgsman, W., 2018. Tangled up in folds: tectonic significance of superimposed folding at the core of the Central Iberian curve (West Iberia). International Geology Review. doi: 10.1080/00206814.2017.1422443

Pastor-Galán, D., Groenewegen, T., Brouwer, D., Krijgsman, W., Dekkers, M.J., 2015a. One or two oroclines in the Variscan orogen of Iberia? Implications for Pangea amalgamation. Geology 43, 527–530. doi:10.1130/G36701.1

Pastor-Galán, D., Gutíerrez-Alonso, G., Dekkers, M.J., Langereis, C., 2018. Paleomagnetism in Extremadura (Central Iberian zone, Spain) Paleozoic rocks: extensive remagnetizations and further constraints on the extent of the Cantabrian orocline. Journal of Iberian Geology 43, 583-600.

Pastor-Galán, D., Gutiérrez-Alonso, G., Mulchrone, K.F., Huerta, P., 2012. Conical folding in the core of an orocline. A geometric analysis from the Cantabrian Arc (Variscan Belt of NW Iberia). Journal of Structural Geology 39, 210–223. doi:10.1016/j.jsg.2012.02.010

Pastor-Galán, D., Ursem, B., Meere, P.A., Langereis, C., 2015b. Extending the Cantabrian Orocline to two continents (from Gondwana to Laurussia). Paleomagnetism from South Ireland. Earth and Planetary Science Letters 432, 223–231. doi:10.1016/j.epsl.2015.10.019

Pereira, M. F., Fernández, R. D., Gama, C., Hofmann, M., Gärtner, A., Linnemann, U., 2017. S-type granite generation and emplacement during a regional switch from extensional to contractional deformation (Central Iberian Zone, Iberian autochthonous domain, Variscan Orogeny). International Journal of Earth Sciences 107, 251-267.

Phillips, W.J., 1974. The dynamic emplacement of cone sheets. Tectonophysics 24, 69–84. doi:10.1016/0040-1951(74)90130-9

Quesada, C., 1991. Geological constraints on the Paleozoic tectonic evolution of tectonostratigraphic terranes in the Iberian Massif. Tectonophysics 185, 225–245. doi:10.1016/0040-1951(91)90446-Y

Ramsay, J.G., 1967. Folding and Fracturing of Rocks. McGraw Hill, New York.

Ramsay, J.G., Huber, M.I., 1987. The techniques of modern structural geology. Volume 2: folds and fractures. Academic Press, London.

Reavy, R.J., 1989. Structural controls on metamorphism and syn-tectonic magmatism: the Portuguese Hercynian collision belt. Journal of the Geological Society of London 146, 649–657. doi:10.1144/gsjgs.146.4.0649

Reavy, R.J., 1988. An investigation into the controls of granite plutonism in the Sierra da Freita region, northern Portugal. University of St. Andrews.

Reber, J.E., Schmalholz, S.M., Burg, J.P., 2010. Stress orientation and fracturing during three-dimensional buckling: Numerical simulation and application to chocolate-tablet structures in folded turbidites, SW Portugal. Tectonophysics 493, 187–195. doi:10.1016/j.tecto.2010.07.016

Reik, G., Currie, J., 1974. A study of relations between rock fabric and joints in sandstone. Canadian Journal of Earth Sciences 11, 1253–1268.

Ribeiro, A., 1990. Central Iberian zone, Introduction. In: Dallmeyer, R.D., Martínez-García, E. (Eds.), Pre-Mesozoic Geology of Iberia, 143–144. Springer-Verlag, Berlin.

Ribeiro, A., Pereira, E., Dias, R., 1990. Structure in the northwest of the Iberian Peninsula. In: Dallmeyer, R.D., Martínez-García, E. (Eds.), Pre-Mesozoic Geology of Iberia, 220-236.

Springer-Verlag, Berlin.

Ries, A.C., Shackleton, R.M., 1976. Patterns of strain variation in arcuate fold belts. Philosophical Transactions of the Royal Society of London. Series A: Mathematical and Physical Sciences 283, 281–288.

Rubio Pascual, F.J., Arenas, R., Martínez Catalán, J.R., Rodríguez Fernández, L.R., Wijbrans, J.R., 2013. Thickening and exhumation of the Variscan roots in the Iberian Central System: Tectonothermal processes and $^{40}Ar/^{39}Ar$ ages. Tectonophysics 587, 207–221. doi:10.1016/j.tecto.2012.10.005

Sequeira, A.J.D., de Sousa, M.B., 1991. O Grupo das Beiras (Complexo Xisto-Grauváquico) da Região de Coimbra-Lousã. Memórias e Noticias, Publicações do Museu e Laboratório Mineralógico e Geológico da Universidade de Coimbra 112, 1–13.

Shaw, J., Johnston, S.T., Gutíerrez-Alonso, G., Weil, A.B., 2012. Oroclines of the Varisican orogen of Iberia : Paleocurrent analysis and paleogeographic implications. Earth and Planetary Science Letters 329-330, 60-70.

Sluijk, D., 1963. Geology and Tin-Tungsten Deposits of the Regoufe Area, Northern Portugal. Universiteit van Amsterdam.

Štemprok, M., 1981. Tin and tungsten deposits of the West-Central European Variscides. In: Proceedings of the Fifth Quadrennial IAGOD Symposium, 495–512.

Talavera, C., Martínez Poyatos, D., González Lodeiro F., 2015. SHRIMP U–Pb geochronological constraints on the timing of the intra-Alcudian (Cadomian) angular unconformity in the Central Iberian Zone (Iberian Massif, Spain). International Journal of Earth Sciences 104, 1739–1757. doi: 10.1007/s00531-015-1171-5

Thadeu, D., 1989. Portugal. In: Dunning, F.W., Garrard, P., Haslam, H.W., Ixer, R.A. (Eds.), Mineral Deposits of Europe. Volume 4/5: Southwest and Eastern Europe, with Iceland, 197-220. The Institution of Mining and Metallurgy and The Mineralogical Society, London.

Twiss, R.J., Moores, E.M., 1992. Structural Geology. W.H. Freeman and Company, New York.

Valle Aguado, B., Azevedo, M.R., Schaltegger, U., Martínez Catalán, J.R., Nolan, J., 2005. U-Pb zircon and monazite geochronology of Variscan magmatism related to syn-convergence extension in Central Northern Portugal. Lithos 82, 169–184. doi:10.1016/j.lithos.2004.12.012

van de Haar, a. J., Vriend, S.P., van Gaans, P.F.M., 1993. Hydrothermal alteration of the Beira schists around the W-Sn specialised Regoufe granite, NW Portugal. Journal of Geochemical Exploration 46, 335–347. doi:10.1016/0375-6742(93)90029-L

Van der Voo, R., Stamatakos, J.A., Parés, J.M., 1997. Kinematic constraints on thrust-belt curvature from syndeformational magnetizations in the Lagos del Valle Syncline in the Cantabrian Arc, Spain. Journal of Geophysical Research: Solid Earth 102, 10105–10119. doi:10.1029/97JB00263

Vriend, S.P., Oosterom, M.G., Bussink, R.W., Jansen, J.B.H., 1985. Trace-element behavior in the W-Sn granite of Regoufe, Portugal. Journal of Geochemical Exploration 23, 13–25.

Wagner, R.H., Álvarez-Vázquez, C., 2010. The Carboniferous floras of the Iberian Peninsula: A synthesis with geological connotations. Review of Palaeobotany and Palynology 162, 239–324. doi:10.1016/j.revpalbo.2010.06.005

Weil, A. B., Gutiérrez-Alonso, G., Johnston, S.T., Pastor-Galán, D., 2013. Kinematic constraints on buckling a lithospheric-scale orocline along the northern margin of Gondwana: A geologic synthesis. Tectonophysics 582, 25–49. doi:10.1016/j.tecto.2012.10.006

Weinberger, R., Eyal, Y., Mortimer, N., 2010. Formation of systematic joints in metamorphic rocks due to release of residual elastic strain energy, Otago Schist, New Zealand. Journal of Structural Geology 32, 288–305. doi:10.1016/j.jsg.2009.12.003

Zhao, M., Jacobi, R.D., 1997. Formation of regional cross-fold joints in the northern Appalachian Plateau. Journal of Structural Geology 19, 817–834. doi:10.1016/S0191-8141(97)00009-6

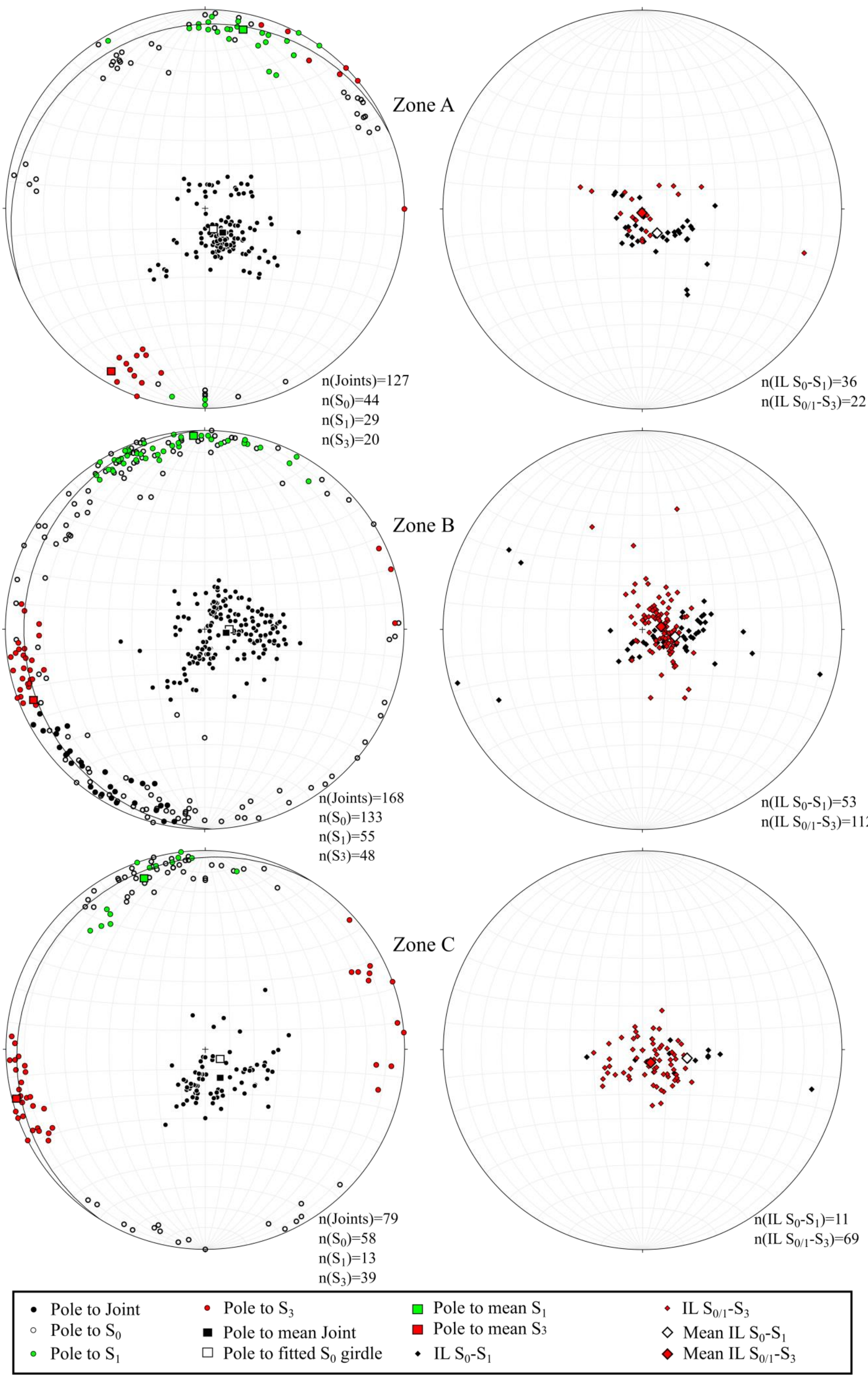

Zone A
n(Joints)=127
n(S_0)=44
n(S_1)=29
n(S_3)=20
n(IL S_0-S_1)=36
n(IL $S_{0/1}$-S_3)=22
Zone B
n(Joints)=168
n(S_0)=133
n(S_1)=55
n(S3)=48
n(IL S_0-S_1)=53
n(IL $S_{0/1}$-S_3)=112
Zone C
n(Joints)=79
n(S_0)=58
n(S_1)=13
n(S_3)=39
n(IL S_0-S_1)=11
n(IL $S_{0/1}$-S_3)=69
Pole to Joint
Pole to S_0
Pole to S_1
Pole to S_3
Pole to mean Joint
Pole to fitted S_0 girdle
Pole to mean S_1
Pole to mean S_3
IL S_0-S_1
IL $S_{0/1}$-S_3
Mean IL S_0-S_1
Mean IL $S_{0/1}$-S_3

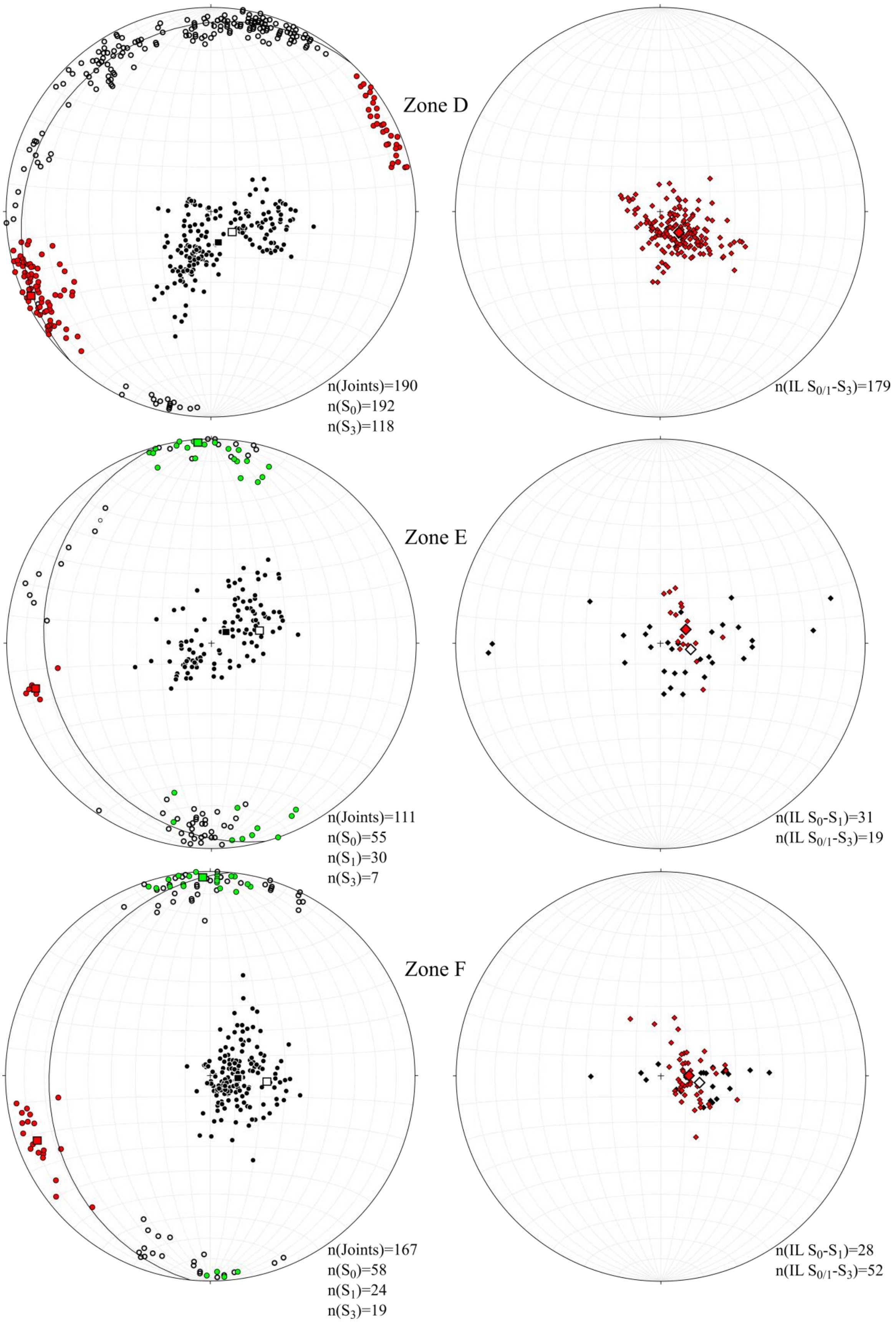
Zone D
n(Joints)=190
n(S_0)=192
n(S_3)=118
n(IL $S_{0/1}$-S_3)=179
Zone E
n(Joints)=111
n(S_0)=55
n(S_1)=30
n(S_3)=7
n(IL S_0-S_1)=31
n(IL $S_{0/1}$-S_3)=19
Zone F
n(Joints)=167
n(S_0)=58
n(S_1)=24
n(S_3)=19
n(IL S_0-S_1)=28
n(IL $S_{0/1}$-S_3)=52

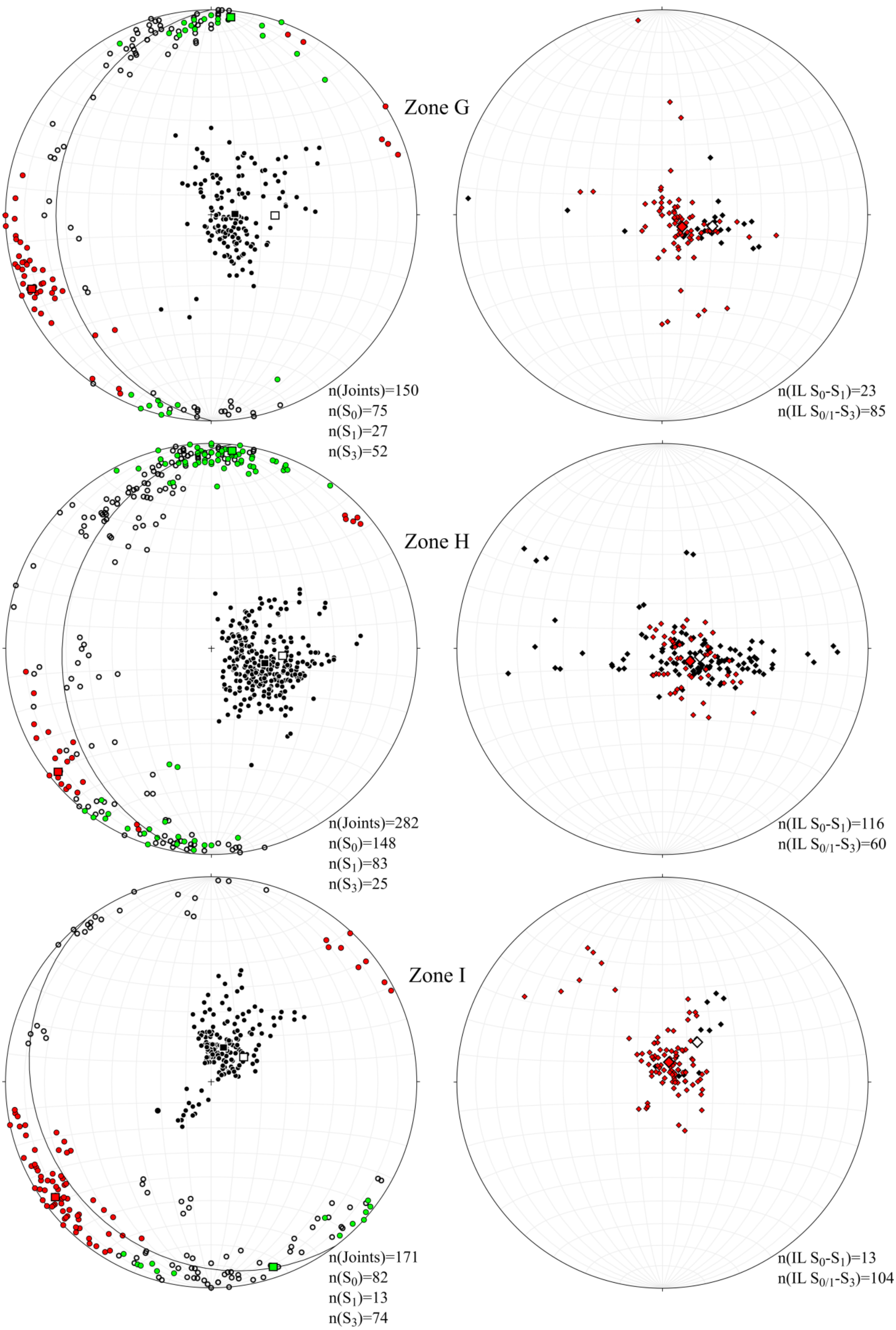
Zone G
n(Joints)=150
n(S_0)=75
n(S_1)=27
n(S_3)=52
n(IL S_0-S_1)=23
n(IL $S_{0/1}$-S_3)=85
Zone H
n(Joints)=282
n(S_0)=148
n(S_1)=83
n(S_3)=25
n(IL S_0-S_1)=116
n(IL $S_{0/1}$-S_3)=60
Zone I
n(Joints)=171
n(S_0)=82
n(S_1)=13
n(S_3)=74
n(IL S_0-S_1)=13
n(IL $S_{0/1}$-S_3)=104

Appendix A.1. Lower-hemisphere, equal-area stereographic projections showing the orientation data collected for zones A-I. For each zone, the poles to the joints, to S_0, to S_1 (not parallel to S_0), to S_3, as well as their mean orientations, are indicated on the left-hand side. On the right-hand side, the S_0-S_1 and $S_{0/1}$-S_3 intersection lineations are indicated.

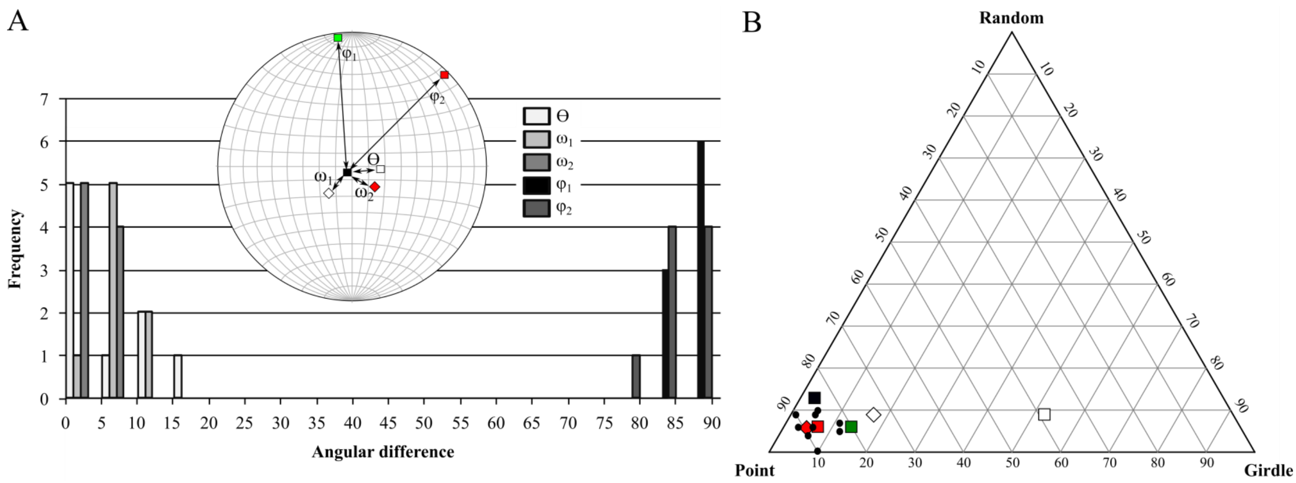

Appendix A.2. Statistical analysis of the mean orientation for zones A-J, added in Table 1. (A) Histogram of the calculated spherical angles θ (angle between the mean of poles to joints and the pole to best-fit girdle to S_0), φ_1 (angle between the means of poles to joints and S_1), φ_2 (angle between the means of poles to joints and S_3), ω_1 (angle between the mean of poles to joints and the mean S_0-S_1 intersection lineation) and ω_2 (angle between the mean of poles to joints and the mean $S_{0/1}$-S_3 intersection lineation). (B) Ternary diagram showing the statistical distribution of the joints (black dots) for each zone, all joints (black square), all measured bedding planes (white square), all measured S_1 and S_3 foliations (green and red square, respectively) and all S_0-S_1 and $S_{0/1}$-S_3 intersection lineations (white and red diamond, respectively).